2017

Theoretical Analysis & Practical Implementation of a Super-Regenerative Receiver for Amplitude Modulated Radio Signals

Anthony Michael Evelina
Lehigh University

Theoretical Analysis & Practical Implementation of a Super-Regenerative Receiver for Amplitude Modulated Radio Signals

By

Anthony M. Evelina Jr.

A Thesis

Presented to the Graduate and Research Committee

Of Lehigh University

In Candidacy for the Degree of

Master of Science

in

Electrical Engineering

Lehigh University

December 2017

Thesis is accepted and approved in partial fulfillment of the requirements for the Master of Science in Electrical Engineering.

Theoretical Analysis & Practical Implementation of a Super-Regenerative Receiver for Amplitude Modulated Radio Signals

Anthony M. Evelina Jr.

_____

Date Approved

_____

Douglas R. Frey (Advisor)

_____

Chengshan Xiao (Department Chair)

Acknowledgements

First and foremost, I would like to express my deep respect and gratitude to my parents for their unconditional love and support throughout my academic career. I am forever grateful for the opportunities they have granted me, and I would like to dedicate my accomplishments with this project to them.

Furthermore, I would like to express my sincere gratitude to my thesis and graduate advisor, Professor Douglas Frey. His influence and teachings throughout my undergraduate studies at Lehigh fully inspired me to pursue a higher education and work towards a Master's of Science in Electrical Engineering. He has consistently challenged me to improve myself as an engineer both in and out of the classroom, which encouraged me to take on this project in the first place. I attribute my successes here at Lehigh and my continuously growing passion for engineering to him and I am truly appreciative of his guidance throughout my time spent here.

Table of Contents

List of Tables & Figures

Abstract

The Super-Regenerative Receiver invented by Edwin Armstrong in 1922 provides simple but effective reception and amplification of modulated radio signals. Despite its age and the increased complexity of communication systems over the years, Super-Regenerative Receivers still find use in various specialized applications due to the simplicity and low-power consumption of the design. This paper aims to provide a thorough mathematical analysis of Super-Regenerative Receivers applied to both a system level model and an electrical band pass circuit while offering a practical implementation for receiving amplitude modulated signals to be compared with simulated results.

Chapter 1

Introduction

1.1 Brief history of the Super-Regenerative Receiver

The Super-Regenerative Receiver (SRR) has been used in a wide variety of wireless communication applications since its invention by Edwin Armstrong in 1922. Throughout the years where vacuum tubes were still prominent in communication circuits, SRRs were an economical and sufficient option for both AM and FM radio implementations and were widely used in commercial walkie-talkie communication devices and military radar identification systems. As transistors began to replace vacuum tubes and receivers with improved selectivity were designed, the SRR withheld prominence in specific applications that call for minimal size and cost at the expense of limited performance.

Currently, SRRs still find use in short-distance radio frequency links that require low cost and low power consumption. These applications include sensor networks, home automation and security systems, and remote-controlled devices such as wireless door openers and radio-controlled toys.

1.2 Principle of Regeneration

The Super-Regenerative Receiver (SRR) is based on Armstrong's previous invention of the Regenerative Receiver in 1912. By definition, a regenerative circuit is one that makes use of positive feedback (regeneration) to send a portion of the output back to the input in phase to reinforce the signal amplitude. In a regenerative scheme, the amount of regeneration or feedback is set to some constant level that achieves maximum

sensitivity to desired input signals while just below the threshold level sufficient for the system to respond to unwanted input noise. In contrast, the level of regeneration in an SRR varies periodically, allowing much higher gains for a portion of time followed by a period of reduced gain. By varying the level of regeneration, higher gains are achievable to increase the systems sensitivity while still retaining sufficient selectivity. The benefit of employing positive feedback is that a minimal number of components with inherently low gain can be configured in a way such that the overall system produces much larger gains. In effect, this minimizes the cost, complexity and size of a receiver implementation, which explains why the SRR is still an attractive option for specialized applications.

Figure 1-1 depicts the block diagram of a classical SRR that will be referenced throughout this paper. In the proceeding chapter, the functionality of each component will be analyzed and described on a system level while reviewing basic concepts of modulation and feedback. This will offer a concise overview to prepare for a deeper mathematical analysis of the systems operation in Chapter 3.

Figure 1-1. Block Diagram of the Classical Super-Regenerative Receiver.

Chapter 2

Super-Regenerative Operation & Review of Relevant Concepts

2.1 SRR Input Stage & Review of Amplitude Modulation

The input stage of an SRR consists of a receiving antenna and a Low-Noise Amplifier (LNA). The LNA at the front end provides isolation between the RF oscillations of the super-regenerative Oscillator's input stage and the receiving antenna. Super-regenerative operation does not depend on the LNA, but its inclusion prevents unwanted re-radiation of the SRO signal back to the input antenna.

SRRs are capable of receiving both amplitude and angle modulated signals, but are predominantly used in amplitude modulated communication applications. In an amplitude modulation scheme, the amplitude of a high frequency carrier signal is varied in proportion to the amplitude of a lower frequency baseband signal. The baseband or message signal contains useful transmitted information which could be in the form of a continuous wave such as an audio signal, or a discrete digital signal. To generate an AM signal, the carrier signal is multiplied by a message signal of some amplitude A_m with an added DC component as shown by:

$$m(t) = A_m \cos(\omega_m t) \quad (2.1)$$
$$c(t) = A_c \cos(\omega_c t) \quad (2.2)$$
$$s(t) = [1 + m(t)] * c(t) \quad (2.3)$$
$$s(t) = A_c \cos(\omega_c t) + \frac{A_c A_m}{2}[\cos((\omega_c - \omega_m)t) + \cos((\omega_c + \omega_m)t)]. \quad (2.4)$$

For successful reception of the signal, it is necessary for $1 + m(t)$ to always be positive, implying that for an arbitrary amplitude, the message signal must never drop below zero. As an example, we shall assume this condition is satisfied and the message signal is a

simple low frequency sinusoid. The result of multiplying these signals is shown by the compound waveform in Figure 2-1.

As seen in Figure 2-1a, the compound waveform of this example consists of three different frequency components which are depicted in the frequency spectrum shown in Figure 2-1b. In effect, the frequency information from the message signal is shifted from the baseband to the higher carrier frequency and reflected across the axis of f_c, resulting in a total bandwidth of $2f_m$. To extract the intended message from the transmitted high frequency signal, radio receivers must demodulate the compound waveform and shift the message back to the baseband. In a simplified sense, this is accomplished by multiplying the sinusoidal signal coupled to the antenna by a sinusoid of the same carrier frequency. By applying the same results of sinusoidal multiplication from (2.3) and (2.4), demodulation produces a new copy of the message signal shifted back to the baseband and another copy residing at twice the carrier frequency. Routing this output to a low pass filter will isolate the message signal at the baseband and suppress the copies at higher frequencies, effectively recovering the intended information.

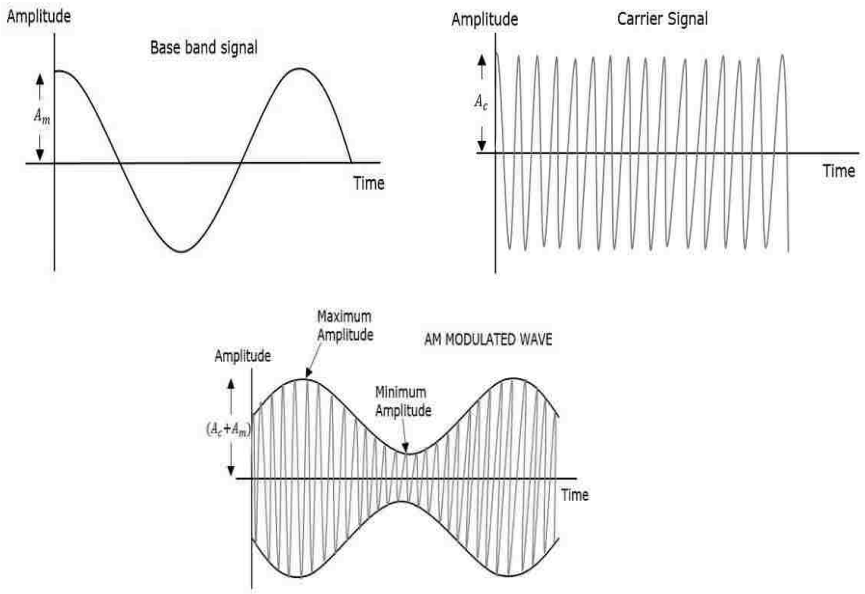

Figure 2-1a. Message Signal (Left), Carrier Signal (Right), and Compound Waveform after Multiplication (Bottom).

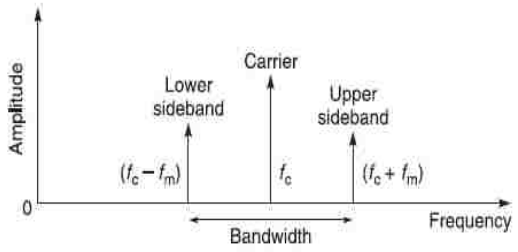

Figure 2-1b. Frequency Representation of Compound waveform in 2-1a.

2.2 Super-Regenerative Oscillator & Review of Feedback

Like most radio receiver architectures, SRRs utilize a sinusoidal oscillator that is set to oscillate at the carrier frequency of the received signal. The *Super-Regenerative Oscillator* (SRO), also known as a positive feedback oscillator, is the defining component of an SRR and governs the receivers operation and performance.

As seen in Figure 1-1, the basic structure of SRO oscillator consists of a frequency selective network and an amplifier in a positive feedback configuration. The frequency selective network is a band pass filter whose impulse and frequency response are given in Figure 2-2.

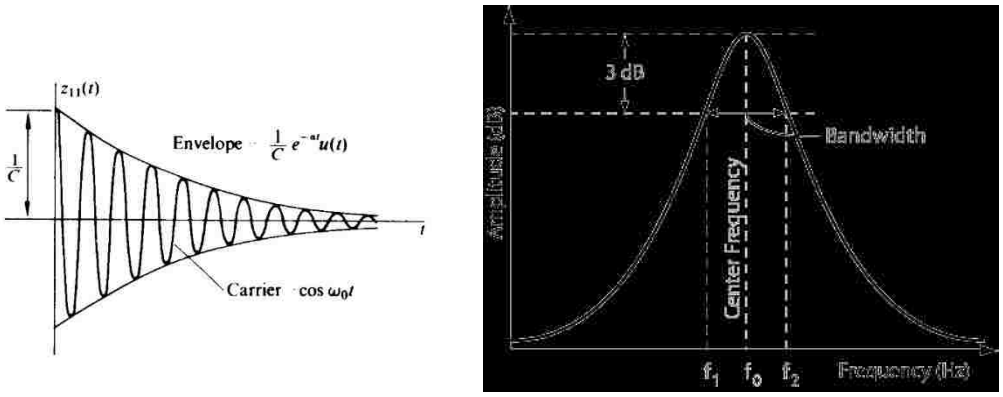

Figure 2-2. (a) Impulse Response and (b) Frequency Response of Band Pass Filter.

Physically this implies that in the presence of an applied impulse at the input, the tuned circuit will ring at its resonant frequency characterized by the center frequency of the filters passband. When there lacks a continued supply of energy to the network at its resonant frequency, these oscillations will decay exponentially as the energy within the network dissipates. By utilizing positive feedback, the decaying oscillatory response from the initial excitation can be reinforced, allowing a constant level dictated by the feedback gain.

When the selective network and amplifier are connected in a positive feedback configuration, the relationship between each signal path is governed by

$$v_o = Bv_s \tag{2.5}$$
$$v_a = K_a v_o \tag{2.6}$$
$$v_S = v_{in} + K_a v_o \tag{2.7}$$

where B is the frequency response of the selective network. Rearranging these equations allows us to relate the output of the system to its input by

$$\begin{aligned} v_o &= \frac{B}{1-K_aB} v_{in} \\ &= \frac{B}{1-L} v_{in} \\ &= H v_{in} , \end{aligned} \tag{2.8}$$

where L is the open loop gain and H is the closed loop gain of the system.

In practice, oscillator circuits are generators and thus have zero input ($v_{in} = 0$), so it may not be initially obvious from (2.8) how such a circuit could start and sustain oscillations. Theoretically for the system to oscillate with zero input, the closed loop gain H must be infinite, implying that the open loop gain $L = K_aB$ must be real with zero phase and unit magnitude. This requirement for steady oscillation is known as the Barkhausen Criterion described in [13]. When the open loop gain is less than unity, the oscillations in the circuit will eventually cease. Conversely, if the open loop gain is greater than unity, the system becomes unstable and the oscillations will theoretically rise to ever increasing levels. In practice however, non-linear characteristics of the gain element cause the open loop gain to shift towards unity as the amplitude approaches a maximum equilibrium value dependent on the gain element.

The distinguishing characteristic of SRRs is that their loop gain is manipulated such that it varies periodically between levels that are higher and lower than unity. Referring to Figure 1-1, the gain of the amplifier K_a in the feedback path is controlled by a time-varying "quench" signal. As the feedback gain varies proportionally with the applied quench signal, the system alternates between states of stability and instability, causing oscillations to build and decay (or quench) in correspondence with the gain level. Thoughtful design of the receiver can allow for "self-quenching" in which the gain

element is automatically controlled, but for a manageable linear analysis of the system in Section 3, it is assumed that the gain is controlled externally by an oscillating quench signal with frequency f_q. In the presence of an RF input, the SRO outputs a series of RF pulses with a period of $T_q = 1/f_q$ until the input signal ceases. In a sense, these pulses can be viewed as "analog samples" of the received input signal.

SRRs have two modes of operation with respective advantages for different communication and modulation schemes. In the *linear-mode* of operation, the oscillations are damped before they reach their equilibrium amplitude characterized by the SRO design. Thus, the level of the output pulses are proportional to the amplitude envelope of the input signal, which is a desirable result for demodulating AM signals. Feeding these pulses through a simple envelope detector and a low pass filter to remove the high frequency quench component effectively demodulates the received signal. In the *logarithmic-mode* of operation, the amplitude of the oscillations reaches its limit before they are damped, resulting in a saturated output every cycle. In this scheme, the output pulses are no longer proportional to the amplitude of the input envelope. Rather, the area under the output pulse is proportional to the logarithm of the amplitude of the input. The constant amplitude of pulses makes the logarithmic mode suitable for digital modulation schemes such as PWM. Though the mathematical analysis presented in proceeding sections focuses on the linear mode of operation, deeper analysis of the logarithmic mode can be found in [1] and [11].

2.3 Detecting the SRO Output & Review of Demodulation

Upon reception of an AM signal that oscillates at the selective networks tuned frequency, the SRR will output a series of evenly spaced high-frequency pulses with peek amplitudes proportional to the message signal amplitude at that instance of time. Any network connected to the receiver would only be interested in the information contained in the message signal, and so the receiver must demodulate the signal by extracting the message from its high frequency carrier.

To recover the message signal, we shall consider the very simple but popular method of non-coherent envelope detection described in [9] and depicted in Figure 2-3.

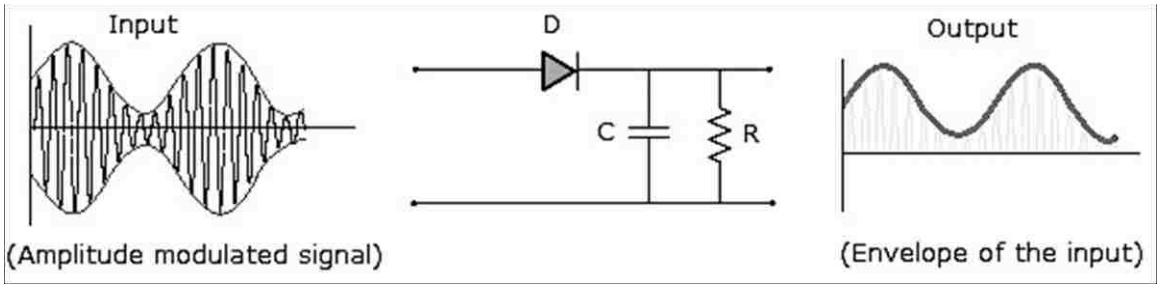

Figure 2-3a. Simple Envelope Detector for AM Signals.

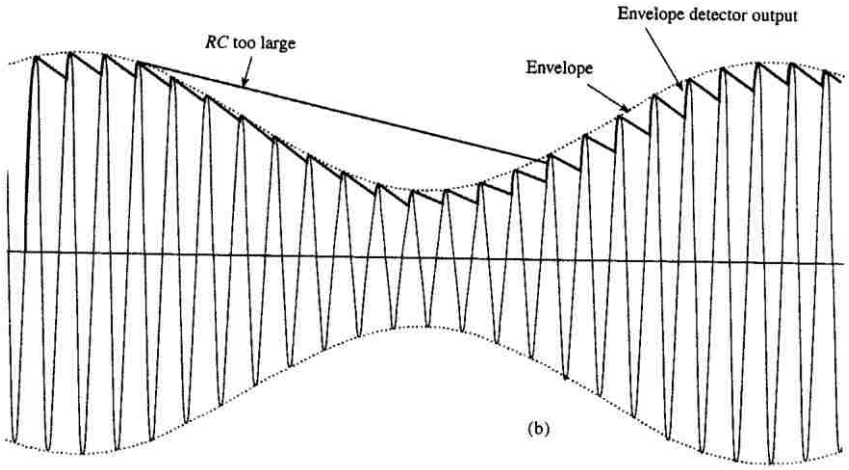

Figure 2-3b. Magnified View of Envelope Detector Output.

During the positive cycle of the input signal, the diode is forward-biased which allows the capacitor to charge to the peak voltage of the input signal. As soon as the input level drops below its peak, the diode becomes reverse-biased and acts as an open circuit. The capacitor then discharges through the resistor at a slow rate with a time constant $\tau = RC$, slowly reducing the voltage across the capacitor. When the input signal becomes positive with respect to the capacitor voltage, the diode is once again forward biased and the process repeats.

In effect, the voltage across the capacitor roughly follows the envelope of the input signal with a small amount of ripple of frequency f_c due to the carrier wave. This high frequency ripple can be reduced by increasing the time constant such that the capacitor discharges less between positive cycles. However, increasing the time constant too much will hinder the capacitors ability to accurately follow the envelope as can be seen in Figure 5b. Thus, time constant τ should be large in comparison to $1/2\pi f_c$, but small compared to $1/2\pi BW$ where BW is the highest frequency within the message signal. Considering the RC network is simply a first order low-pass filter, higher-order filtering of greater complexity can be employed to provide a steeper cutoff and further minimize unwanted high-frequency ripple.

Chapter 3

Mathematical Analysis of the Classical SRR

This section offers a solution the characteristic equation of the SRR to be applied to specific cases of operation in the following section. Additionally, this section defines a new set of parameters that characterize the systems performance and simplify the mathematical analysis of the solution. The proceeding mathematical derivations are based on the results found in [1] and may be compared to an alternative state-space representation of the system presented in [6] and [7].

3.1 Characteristic Equation of SRR

Since practical SRRs are non-linear devices, the mathematics describing their operation makes numerous assumptions and approximations to linearize the equations and present elegant and understandable results for different cases of operation. To begin our mathematical approach, we shall assume that the SRO is operating in the linear mode. The band pass network has a response centered at frequency $\omega_0 = 2\pi f_0$, characterized by the generic second-order band pass transfer function:

$$H_{bpf}(s) = K_0 * \frac{2\zeta_0\omega_0 s}{s^2+2\zeta_0\omega_0 s+\omega_0^2} \tag{3.1}$$

Converting this transfer function to the time domain produces the equivalent differential equation

$$\ddot{v}_o(t) + 2\zeta_0\omega_0\dot{v}_o(t) + \omega_0^2 v_o(t) = K_0 2\zeta_0\omega_0\dot{v}_s(t) \tag{3.2}$$

where K_0 denotes the maximum amplification of the network and ζ_0 represents the quiescent damping factor. Without feedback, the value of each variable is fixed and dependent on the design of the filter. The output of the band pass filter is fed back to its input establishing the relationship:

$$v_s(t) = v_{in}(t) + K_a(t)v_o(t). \tag{3.3}$$

By substituting this expression for $v_s(t)$ into (3.1), we obtain the closed loop transfer function and corresponding linear differential equation:

$$H_{SR}(s,t) = K_0 * \frac{2\zeta_0\omega_0 s}{s^2+2\zeta(t)\omega_0 s+\omega_0^2} \tag{3.4}$$

$$\ddot{v}_o(t) + 2\zeta_0\omega_0\dot{v}_o(t) + \omega_0^2 v_o(t) = K_0 2\zeta_0\omega_0[\dot{v}(t) + K_a(t)v_o(t)] \tag{3.5}$$

$$\ddot{v}_o(t) + 2\zeta(t)\omega_0\dot{v}_o(t) + \omega_0^2 v_o(t) = 2\zeta_0\omega_0\dot{v}(t). \tag{3.6}$$

When the loop is closed, the damping factor ζ becomes a time-varying signal

$$\zeta(t) = \zeta_0 * \left(1 - K_0 * K_a(t)\right) \tag{3.7}$$

$$= \zeta_0 - \zeta_0 K_0 K_a(t) \tag{3.8}$$

$$= \zeta_{dc} + \zeta_{ac}(t) \tag{3.9}$$

This damping function plays a critical role in the design and analysis of super-regenerative receivers, as many measurable and adjustable performance parameters are dependent on it.

3.2 Damping Function

The time-varying damping function characterizes the systems sensitivity – and thus, its oscillatory response – to an input signal. One damping cycle corresponds to one quench cycle with a period of $T_q = 1/f_q$. Depending on the value of $\zeta(t)$ during this period, the system response can be undamped ($|\zeta| = 0$) underdamped ($|\zeta| < 1$), critically damped ($|\zeta| = 1$), or over damped($|\zeta| > 1$). Figure 3-1 from [12] depicts how

the pole-zero plot of the system is affected by a linearly decreasing damping function. This shall be viewed as a single cycle of a saw tooth quench signal with a time interval of $[t_a, t_b]$.

Figure 3-1. Effect of a Varying Damping Ratio on Pole-Zero Plot of SRO.

To demonstrate how the damping function affects the systems response in the time domain, consider the sinusoidal damping function in Figure 3-2 from [1] with an equivalently defined quench interval $[t_a, t_b]$. As $\zeta(t)$ approaches zero, the poles of the system shift closer to the right half plane of the Laplace domain. The receiver is most sensitive to input signals at this time and the presence of an input around this time will cause an output response. When the damping function drops below zero, the poles cross the imaginary axis into the right-half plane causing the system to become unstable. Within the interval of the negative portion of the damping function $[0, t_b]$, the system gain increases significantly, causing an output pulse $p_o(t)$ to rise exponentially. Then, as the damping factor undergoes the positive half cycle, the poles shift back towards the left-hand plane, decreasing the systems sensitivity to an input while quenching the RF energy buildup from the unstable portion of the cycle.

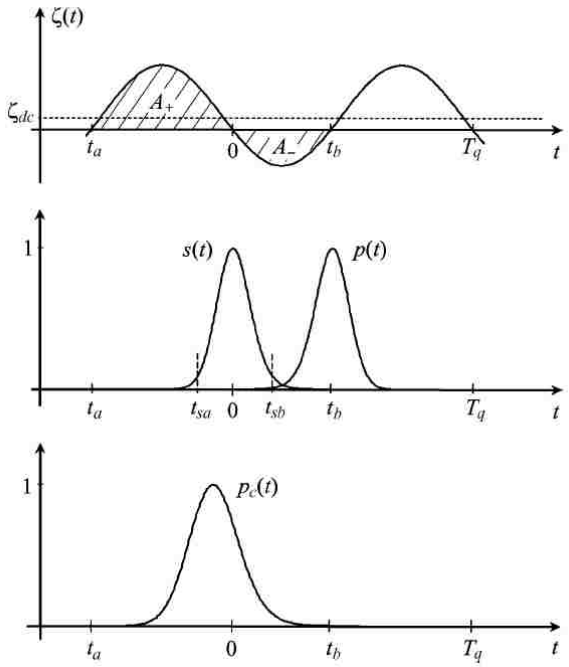

Figure 3-2: (a) Sinusoidal Damping function, (b) sensitivity and output curves, (c) applied RF input pulse envelope.

If we define t_o to be the time at which the damping function becomes negative, we see that ζ_{DC} essentially dictates the amount of time the system is in a damped ($t_a < t < t_0$) and undamped ($t_0 < t < t_b$) state. The longer the damping factor is positive, the more time is allowed for the poles to sit in the left-hand plane to let the output sufficiently decay before the next cycle. On the other hand, the negative portion of the damping factor should be long enough to allow the output to rise to a sufficient signal level for detection. In practice, any arbitrary wave function can be chosen so long as it provides sufficient regeneration and quenching by having appropriately sized positive and negative portions within each cycle.

3.3 Sensitivity

As previously mentioned, the value of $\zeta(t)$ during a quench period dictates the sensitivity of the receiver to an input signal. The level of sensitivity is inversely proportional to the minimum received signal level necessary to generate an output, and the width of the sensitivity envelope defines the duration for which the SRR is influenced by that received excitation as explained in [10]. The level of sensitivity exhibits an exponential dependence on the damping function, quantitatively expressed as

$$s(t) = e^{\omega_0 \int_0^t \zeta(\lambda) d\lambda}. \tag{3.10}$$

The sensitivity of the receiver peaks at $t = 0$ when the system is in an undamped state and decreases exponentially as time departs from the origin on both sides. When an input pulse p_{in} occurs within this period of high sensitivity, an output pulse will occur at the end of the cycle. The decaying portion of the output pulse envelope is described by the equation:

$$p_o(t) = e^{-\omega_0 \int_{t_b}^t \zeta(\tau) d\tau}. \tag{3.11}$$

It should be noted that when sensitivity is high, even the smallest excitation such as thermal noise of electrical components can push the system into oscillation, even when there is no appreciable input signal present. However, the smaller the excitation, the longer it will take for oscillations to build. Thus, the sensitivity period of the receiver should be long enough to present sufficient gains in the presence of an input, but quick enough to suppress the slower building oscillations due to electrical noise - A condition that is dictated by the frequency of the applied quenching signal.

3.4 Solution of the Differential Equation

Assuming a linear mode of operation, the general solution to the second order differential equation (6) can be represented as the sum of the homogenous and particular solutions according to

$$v_o(t) = v_{oH}(t) + v_{oP}(t). \tag{3.12}$$

The term $v_{oH}(t)$ represents the natural (or free) response, which may exist without the presence of an input, and $v_{oP}(t)$ represents the forced response due to an input excitation.

3.4.1 Homogenous Solution: Free Response

To solve for the homogeneous response, we first set the input$v(t) = 0$, resulting in the homogenous equation

$$\ddot{v}_{oH}(t) + 2\zeta_0\omega_0\dot{v}_{oH}(t) + \omega_0^2 v_{oH}(t) = 0\ . \tag{3.13}$$

To simplify analysis, we make the following change of variable from $v_{oH}(t)$ to $u(t)$

$$v_{oH}(t) = u(t)e^{-\omega_o\int_{t_a}^{t}\zeta(\lambda)d\lambda} \tag{3.14}$$

$$\dot{v}_{oH}(t) = (\dot{u} - \omega_o\zeta(t) * u)e^{-\omega_o\int_{t_a}^{t}\zeta(\lambda)d\lambda} \tag{3.15}$$

$$\ddot{v}_{oH}(t) = \left(\ddot{u} - 2\omega_o\zeta(t)\dot{u} + \left[\left(\omega_0\zeta(t)\right)^2 - \omega_0\dot{\zeta}(t)\right]u\right)e^{-\omega_0\int_{t_a}^{t}\zeta(\lambda)d\lambda}, \tag{3.16}$$

and substitute these expressions into the original equation. This substitution converts the homogeneous equation into the Hill Equation as shown in [1]:

$$\ddot{u}(t) + \omega_0^2\left(1 - \zeta^2(t) - \frac{\dot{\zeta}(t)}{\omega_0}\right)u(t) = 0. \tag{3.17}$$

To simplify this equation and further analysis, we must satisfy two restrictions imposed on the damping function:

$$\zeta^2(t) \ll 1 \tag{3.18}$$

$$|\dot{\zeta}(t)| \ll \omega_0. \tag{3.19}$$

The first restriction implies that the instantaneous damping factor must be low enough such that the system is underdamped and capable of generating an oscillatory response. Considering the quality factor Q of the system where

$$Q(t) = \frac{1}{2\zeta(t)}, \tag{3.20}$$

this restriction equivalently implies that the quality factor (or the frequency selectivity) $Q(t)$ of the network must be kept high. As shown in Figure 3-3, a low quality factor corresponds to a wide receiver bandwidth, making the system more susceptible to signals and noise outside the bandwidth of interest.

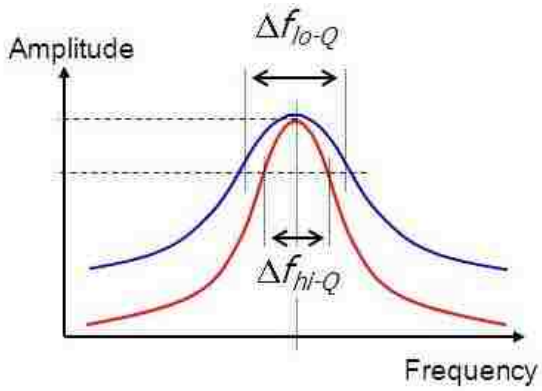

Figure 3-3. Frequency response of a High-Q (Red) and Low-Q (Blue) System.

The second restriction implies that the damping factor must be slow varying compared to the input RF frequency. Since the damping factor varies at a rate of f_q, this restriction equivalently states that the quench frequency f_q should be much lower than the center frequency of the selective band pass network f_0. Satisfying these two restrictions reduces the Hill equation to:

$$\ddot{u}(t) + \omega_0^2 u(t) = 0. \tag{3.21}$$

As can be seen, this representation of the system is linear with constant coefficients unlike our original expression in (6). The solution to this equation will not be derived in this paper, though it is known to be:

$$u(t) = 2Re\left[V_1 e^{j\omega_0 t}\right] = V_1 e^{j\omega_0 t} + V_2 e^{-j\omega_0 t}. \tag{3.22}$$

Substituting this expression (3.22) into (3.21) and reversing the change of variables made in (3.14), (3.15), and (3.16) provides the general solution to the homogenous differential equation:

$$v_{oH}(t) = e^{-\omega_0 \int_{t_a}^{t} \zeta(\lambda) d\lambda} * 2Re\left[V_1 e^{j\omega_0 t}\right]. \tag{3.23}$$

3.4.2 Particular Solution: Forced Response

To find the particular solution of the equation, we begin by using the method of variation of parameters as described in [1]:

$$v_{oP}(t) = 2Re[V_2(t)b(t) + V_2^*(t)b^*(t) \tag{3.24}$$

$$b(t) = e^{-\omega_0 \int_{t_a}^{t} \zeta(\lambda) d\lambda} e^{j\omega_0 t}. \tag{3.25}$$

According to the method of variation of parameters, the particular solution satisfies the complete equation if

$$\dot{V}_2 b + \dot{V}_2^* b^* = 0 \tag{3.26}$$

$$\dot{V}_2 \dot{b} + \dot{V}_2^* \dot{b}^* = 2K_0 \zeta_0 \omega_0 \dot{v}. \tag{3.27}$$

Solving this system of equations for $\dot{V}_2$ yields the expression

$$\dot{V}_2(t) = -jK_0 \zeta_0 \frac{\dot{v}(t)}{b(t)}. \tag{3.28}$$

Integrating both sides of (3.28) provides an expression for V_2

$$\begin{aligned} V_2(t) &= -jK_0 \zeta_0 \int_{t_a}^{t} \frac{\dot{v}(\tau)}{b(\tau)} d\tau \\ &= -jK_0 \zeta_0 \int_{t_a}^{t} \dot{v}(\tau)\, e^{\omega_0 \int_{t_a}^{\tau} \zeta(\lambda) d\lambda} e^{-j\omega_0 \tau} d\tau \end{aligned} \tag{3.29}$$

and by substituting (3.29) into (3.24), the expression for the particular solution is obtained:

$$v_{oP}(t) = e^{-\omega_0 \int_{t_a}^{\tau} \zeta(\lambda) d\lambda} \times 2Re\left[-jK_0\zeta_0 \int_{t_a}^{t} \dot{v}(\tau)\, e^{\omega_0 \int_{t_a}^{\tau} \zeta(\lambda) d\lambda} e^{-j\omega_0(\tau - t)} d\tau\right]. \quad (3.30)$$

3.5 Redefining Gain for a Compact Expression of the Complete Solution

Though these solutions are complete, they don't exactly offer an obvious understanding of the systems operation. To offer a better interpretation of these equations, we may re-write them as a product of several parameters that characterize the systems performance while reducing the mathematical complexity of the solution.

As mentioned earlier, the gain of the overall system is dependent on the time-varying damping function. The additional gain achieved by closing the loop is typically separated into two parameters that are used to describe the performance of the receiver. Since these gains arise from the positive feedback (or regeneration) of the closed loop, they are referred to as the systems *regenerative* and *super-regenerative gain.*

The *regenerative gain* of the system K_r is dependent on the DC component of the damping factor, the frequencies of the received signal and tuned oscillator, and the area of the input pulse envelope weighted by the sensitivity curve across one quench interval $[t_a, t_b]$:

$$K_r = \zeta_0 \omega \int_{t_a}^{t_b} p_{in}(\tau) s(\tau) d\tau. \quad (3.31)$$

The more concentrated the input pulse energy is centered around peak sensitivity, the higher the resulting regenerative gain. A wider input pulse of equal energy or a pulse occurring away from peak sensitivity will result in a smaller regenerative gain. Note that the expression in (3.31) assumes the input frequency matches the frequency of the

selective network. The dependence on ω shows that a greater number of received RF oscillations within a quench cycle increases the regenerative gain. In other words, during the high sensitivity period each successive RF cycle pushes the output envelop level slightly higher. Thus, more RF cycles (higher frequency signal) within the sensitivity period results in a larger regenerative gain.

The *super-regenerative gain* of the system K_s is characterized by the exponential growth of the oscillation and is determined by the area enclosed by the negative portion of the damping function:

$$K_s = e^{-\omega_0 \int_0^{t_b} \zeta(\tau) d\tau}. \tag{3.32}$$

Since $\zeta(t)$ is negative within$[0, t_b]$, evaluation of the integral produces a positive term in the exponential, showing that K_r is exponentially proportional to the systems period of instability. One could also verify from (3.10) and (3.32) that K_s is defined as the inverse of the sensitivity curve $s(t)$.

It is worth noting that since these two parameters are dependent on the damping function, they are inherently related to the periodic feedback gain $K_a(t)$. The total or peak gain of the system is simply expressed the product of the three defined gains within the system:

$$K = K_0 K_r K_s. \tag{3.33}$$

With these new gain parameters defined, we may substitute them into (3.23) and (3.30) to obtain the following homogenous and particular solutions in compact form:

$$v_{oH}(t) = V_h p(t) \cos(\omega_0 t + \phi_h) \tag{3.34}$$

$$v_{oP}(t) = 2\zeta_0 K_0 K_s p(t) \int_{t_a}^{t} \dot{v}_{in}(\tau) s(\tau) \sin\big(\omega_0 (t-\tau)\big)\, d\tau. \tag{3.35}$$

V_h and ϕ_h are respectively related to the modulus and angle of the complex constant V_1 introduced in **Section 3.1** Now that the complete general solution to the characteristic differential equation has been derived, specific cases related to the practical behavior and performance of a super regenerative receiver can be easily analyzed.

3.5.1 SRR Response to an RF Pulse When Tuned to Carrier Frequency

In practical implementations, the receiver is designed to accept incoming RF signals within the band of interest. With the complete solution clearly defined, we can begin to analyze the case of an applied RF pulse in which the carrier frequency is equal to the center frequency of the tuned band pass filter.

To start, it is assumed the RF pulse is applied within the interval of one quench period $[t_a, t_b]$ with the expression

$$v(t) = Vp_{in}(t)\cos(\omega t + \phi). \tag{3.36}$$

The function $p_{in}(t)$ is the normalized envelope of the incoming RF pulse and V is its peak amplitude. Ideally, $p_{in} = 0$ outside of the defined quench period. Otherwise, a fraction of the input signal received in one quench period will carry over into the next quench period. In other words, the free response v_{oH} during the second quench period will be non-zero, and thus the output will no longer be solely described by the forced response to an input pulse within this period. The effects of a non-zero free response will be explained in later sections, but for now we assume $v_{oi}(t) = v_{oPi}(t)$ for every i^{th} quench period.

From (35), we see that the forced response v_{oP} is related to the derivative of the input excitation, which is defined as

$$\dot{v}_{in}(t) = V[\dot{p}_{in}(t)\cos(\omega t + \phi) - p_{in}(t)\omega \sin(\omega t + \phi)]. \quad (3.37)$$

Assuming the input envelope varies slowly compared to its carrier oscillations ($|\dot{p}_{in}(t)| \ll p_{in}(t)\omega$), we the input signal is approximated as

$$\dot{v}_{in}(t) \approx -Vp_{in}(t)\omega\sin(\omega t + \phi). \quad (3.38)$$

Since the free response v_{oH} is assumed be zero, the substitution of (3.38) into (3.30) provides the output response of the system expressed as

$$v_o(t) \approx -2V\zeta_0 K_0 K_s \omega p(t) \times$$
$$\int_{t_a}^{t} p_{in}(\tau)s(\tau)\sin(\omega\tau + \phi)\sin\big(\omega_0(t-\tau)\big)\,d\tau. \quad (3.39)$$

Since the input and sensitivity envelopes are slow-varying compared to ω, the weight of the high frequency component within the integral will be much lower than the low-frequency component, allowing the approximation

$$v_o(t) \approx -2V\zeta_0 K_0 K_s \omega p(t) \times$$
$$\int_{t_a}^{t} p_{in}(\tau)s(\tau)\cos\big((\omega-\omega_0)\tau + \omega_0 t + \phi\big)\,d\tau. \quad (3.40)$$

Recall that the sensitivity curve $s(t)$ decreases rapidly as t departs from the origin on both sides, reaching negligibly small values outside of the sensitivity period $[t_{sa}, t_{sb}]$ defined in Figure 3-2. Outside of this interval, one can assume the influence of an input pulse on the output is very small. Assuming that $s(t)$ is small at the end of a quench period, the effects of sensitivity on the output envelope and super-regenerative gain can be seen by the expression

$$s(t_b) = p_o(0) = e^{\omega_0 \int_0^{t_b} \zeta(\lambda)d\lambda} = \frac{1}{K_s} \ll 1. \quad (3.41)$$

These relationships imply that a small sensitivity value at the end of a quench cycle ($t = t_b$), results in small output envelope values at $t = 0$ and large super-regenerative gains. This reiterates the fact that the output pulse from one cycle should be quenched before the next high sensitivity period at $t = 0 + T_q$ in the next cycle. With this satisfied, the response is solely dictated by the input signal captured at that time, which is then amplified at the end of the cycle $t = t_b$.

Now, imposing the assumption that the receiver is tuned to the input carrier frequency ($\omega = \omega_0$), the approximate expression for the output (3.40) is simplified to

$$v_o(t) = VK_0K_sp_o(t)\left[\zeta_0\omega_0\int_{t_a}^{t_b} p_{in}(\tau)s(\tau)d\tau\right]\cos(\omega_0 t + \phi)\ . \tag{3.42}$$

Upon closer examination, we can see that factor contained in the brackets is the expression for the previously defined regenerative gain K_r (3.31), allowing an even further simplified expression for the output:

$$\begin{aligned} v_o(t) &= VK_0K_rK_sp_o(t)\cos(\omega_0 t + \phi) \\ &= VKp_o(t)\cos(\omega_0 t + \phi). \end{aligned} \tag{3.43}$$

3.5.2 SRR Response to an RF Pulse of Arbitrary Carrier Frequency

Until this point, it has been assumed that the carrier frequency of the input pulse is equal to the tuned frequency of the SRO. To analyze the systems performance for an arbitrary input carrier frequency, the regenerative gain and its dependence on the input frequency must be considered. The general response to an excitation at an arbitrary carrier frequency ω can then be given as

$$v_o(t) = VKp_o(t)\left(\frac{\omega}{\omega_0}\right) * \frac{\int_{t_a}^{t_b} p_{in}(\tau)s(\tau)\cos((\omega-\omega_0)\tau+\omega_0 t+\phi)d\tau}{\int_{t_a}^{t_b} p_{in}(\tau)s(\tau)d\tau}$$

$$= VKp_o(t)\left(\frac{\omega}{\omega_0}\right) * \frac{Re[(\int_{t_a}^{t_b} p_{in}(\tau)s(\tau)e^{j(\omega-\omega_0)\tau}d\tau)e\hat{}j(\omega_0 t+\phi)]}{\int_{t_a}^{t_b} p_{in}(\tau)s(\tau)d\tau}. \quad (3.44)$$

By defining the complex function

$$\psi(\omega) = \int_{-\infty}^{\infty} p_{in}(t)s(t)e^{j\omega t}dt$$
$$= F^*\{p_{in}(t) * s(t)\} \quad (3.45)$$

where $F[x]$ represents the fourier transform of x, and utilizing the fact that the input pulse $p_{in}(t) = 0$ outside of the interval $[t_a, t_b]$, the output response can be re-written as

$$v_o(t) = VKp_o(t)\left(\frac{\omega}{\omega_0}\right)\frac{Re[\,\psi(\omega-\omega_0)e^{j(\omega_0 t+\phi)}]}{\psi(0)}$$

$$= VKp_o(t)\left(\frac{\omega}{\omega_0}\right)\frac{|\psi(\omega-\omega_0)|}{\psi(0)}\cos(\omega_0 t + \phi + \phi_\psi) \quad (3.46)$$

where ϕ_ψ is the angle of $\psi(\omega - \omega_0)$. By defining the frequency dependent component of the above expression as

$$H(\omega) = \left(\frac{\omega}{\omega_0}\right)\frac{|\psi(\omega-\omega_0)|}{\psi(0)}, \quad (3.47)$$

The output response can be condensed to the expression

$$v_o(t) = VKp_o(t)|H(\omega)|\cos(\omega_0 t + \phi + \phi_H). \quad (3.48)$$

Note that for the case of an incoming RF pulse with carrier frequency $\omega = \omega_0$, the magnitude and angle of the frequency dependent component $H(\omega)$ are 1 and 0° respectively, resulting in a response identical to that of the received pulse in Section 3.5.1.

3.5.3 Response to a Sinusoidal Input

With the response to a single RF pulse defined, the case of a steady sinusoidal input given as

$$v_{in}(t) = Vcos(\omega t + \phi) \quad (3.49)$$

can be explored. To utilize the results from previous sections, this sinusoid can be viewed as a sum of successive RF pulses occurring every m^{th} quench period,

$$v_{in}(t) = V\sum_{m=-\infty}^{\infty} p_{in}\left(t - mT_q\right)\cos(\omega\left(t - mT_q\right) + m\omega T\_q + \phi), \qquad (3.50)$$

where the pulse envelope $p_{in}(t - mT_q)$ is square with unit amplitude [8]. By utilizing (3.48), the total response to (3.49) can be expressed as a superposition of single responses to each m^{th} pulse:

$$v_o(t) = VK|H(\omega)| \times \sum_{m=-\infty}^{\infty} p_o\left(t - mT_q\right)\cos\left(\omega_0 t + m(\omega - \omega_0)T_q + \phi + \phi_h\right). \qquad (3.51)$$

3.6 Hangover

Recall that before this mathematical discussion began, it was assumed that the response v_0 to input pulse p_{in} in a given quench cycle did not affect the response in the next quench cycle. To achieve this ideality, the system must be sufficiently damped at the beginning of a quench period to ensure any remaining energy from past periods is extinguished. Thus, the output oscillation in a given quench cycle depends only on the incoming signal within the sensitivity period of that quench cycle.

Hangover occurs when output oscillation in a given quench cycle is generated from the remnant of the previous cycle. In other words, energy from the previous bit "hangs over" into the next quench cycle. In digital communication schemes, a high level of hangover will result in inter-symbol interference, thus increasing the bit-error rate. In this case, the effects of appreciable hangover in the time domain result in a phenomenon known as *multiple resonance* which affects the frequency response of the system. As the amount of hangover increases, resonant peaks occurring at integer multiples of the

quench frequency become increasingly defined. Examples of these effects from [1] can be seen in Figure 3-4 and Figure 3-5.

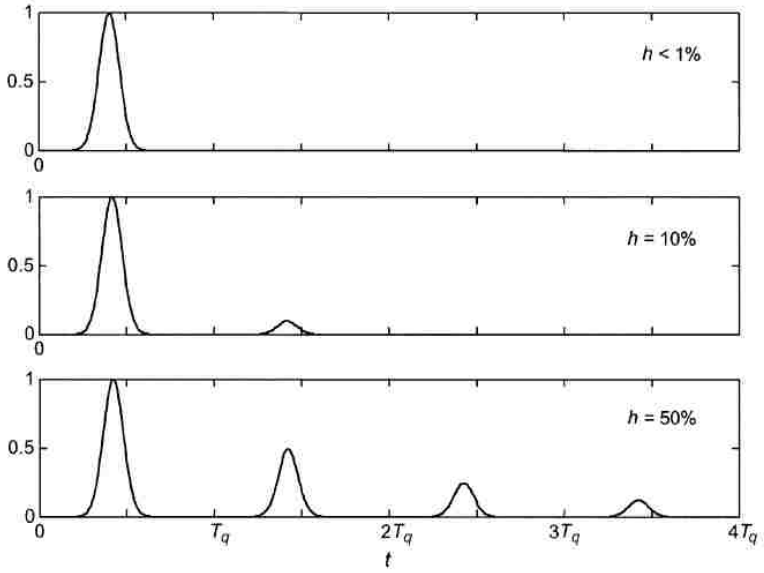

Figure 3-4. SRR Output Pulse Envelope for Different Hangover Percentages.

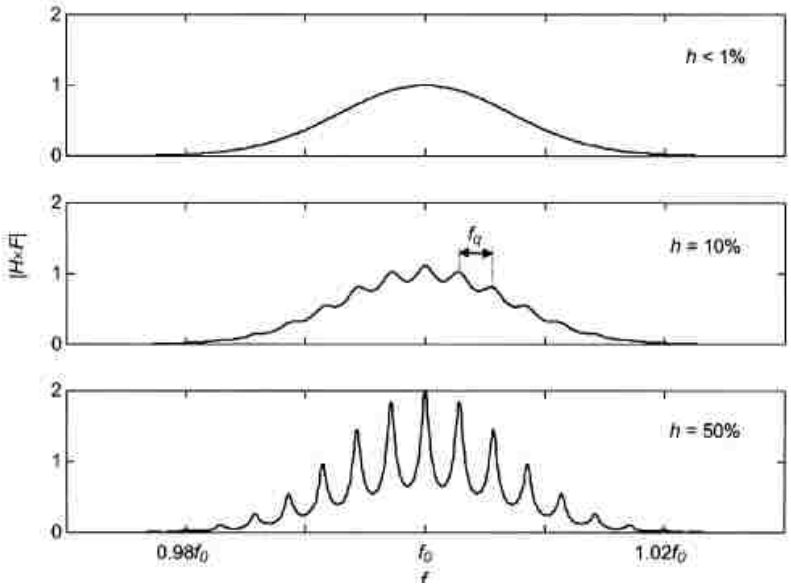

Figure 3-5. Effect of Hangover in the Frequency Response for Different Hangover Percentages (Sinusoidal Steady State).

To quantify this behavior, the hangover coefficient is defined as the ratio between the peak amplitudes of the second output pulse after time T_q and that of the first output pulse

$$p_o(t) = e^{-\omega_0 \int_{t_b}^{t} \zeta(\lambda) d\lambda} = e^{-\omega_0 \zeta_{DC}(t-t_b)} e^{-\omega_0 \int_{t_b}^{t} \zeta_{AC}(\lambda) d\lambda} \tag{3.52}$$

$$h = \frac{p_o(t_b+T_q)}{p_o(t_b)} = e^{-\omega_0 \zeta_{DC} T_q} = e^{\frac{-2\pi\zeta_{DC} f_0}{f_q}}. \tag{3.53}$$

The term $\zeta_{DC} T_q$ is the area enclosed by the mean value of $\zeta(t)$ in one quench cycle, or more simply, the difference in area between the positive and negative portions of the damping function. To minimize hangover, this difference should be maximized while still retaining proper performance. To achieve this practically, compromises have to be made. Raising the dc component of the damping function will reduce hangover but will decrease the frequency selectivity of the system. On the other hand, lowering the quench frequency increases the length of the sensitivity period, resulting in larger regenerative gains that will push practical receivers outside their linear region of operation.

In practice, the quench rate is restricted to a minimum value dictated by the maximum frequency of the modulating message signal. Considering the system is essentially sampling the input every quench cycle, the quench frequency must be at least twice the bandwidth of the modulating signal ($f_q \geq 2BW$) to effectively capture the signal information as given by the Nyquist Sampling Theorem. So, to reduce hangover at a given quench frequency, ζ_{DC} must be increased to satisfy the following condition:

$$\zeta_{DC} > \frac{f_q}{2\pi f_0} \ln\left(\frac{1}{h}\right). \tag{3.54}$$

Chapter 4

Simulation of the Classical SRR

4.1 Simulation Model

The block diagram in Figure 4-1 was created using Matlab's Simulink program to simulate the analytical results obtained in previous sections. This model contains all of the components from our original diagram with the exclusion of the optional Low-Noise Amplifier.

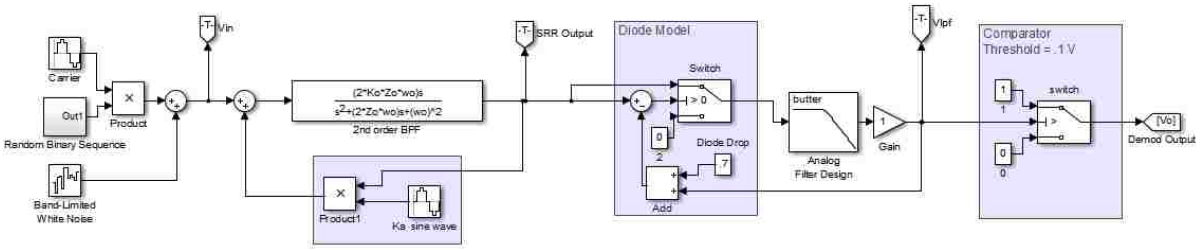

Figure 4-1. Simulink Model of SRR

The input to the SRR is an amplitude modulated sinusoid with frequency f_c equal to the tuned frequency of the filter f_0, modulated by a random binary sequence with bitrate BR. The variable gain amplifier in the feedback loop is modeled simply as the product of the output signal and a sinusoid oscillating at quench frequency f_q with an amplitude equal to the feedback gain K_a. From (3.7) we can derive the time-varying damping function of the system as

$$\zeta(t) = \zeta_0\left[1 - K_0 K_a \sin\left(\omega_q t\right)\right]. \tag{4.1}$$

The output of the SRR is sent to a simple AM envelope detector circuit consisting of a diode and 4th order Butterworth low pass filter for a steep roll-off at a cutoff frequency higher than f_{BR} and lower thanf_q.

4.2 Simulation of Ideal SRR Operation

The design parameters for the ideal simulation and corresponding results are given in Table 4-1 and Figure 4-2. Figure 4-2a shows the ideal amplitude modulated input signal. Received signals in practice are of much lower amplitude, but under appropriate operating conditions the receiver response will be similar to the simulation results on a per unit basis. The output of the SRR is shown in Figure 4-2b. The peeks in the waveform are a result of the damping function reaching an undamped state allowing oscillations to rise. Comparing (a) to (b) it is seen that the overall gain of the SRR is roughly 4.5 V/V – quite low for typical SRR implementations. With careful observation of (4.1), the damping function never actually reaches a value below zero when both K_0 and K_a are unity, implying from (3.32) that the super-regenerative gain of the system is also unity. This implies that the overall gain increase of this simulation is dictated solely by the regenerative gain K_r. Much higher gains are achievable with small increases to K_0 or K_a that allow the damping function to reach a negative value and are in fact necessary for typically low amplitude input signals.

Variables	Sym	Value
Sample Frequency	f_s	10 MHz
Tuned Frequency of BPF	f_0	1 MHz
Carrier Frequency	f_c	1 MHz
Quench Frequency	f_q	40 KHz
Bit Rate	BR	10 Kb/s
Damping Ratio	ζ_0	.1
Open Loop Filter Gain	K_0	1
Feedback Gain	K_a	1
Input Voltage	V	1 V

Table 4-1. Parameters for Ideal SRR Simulation.

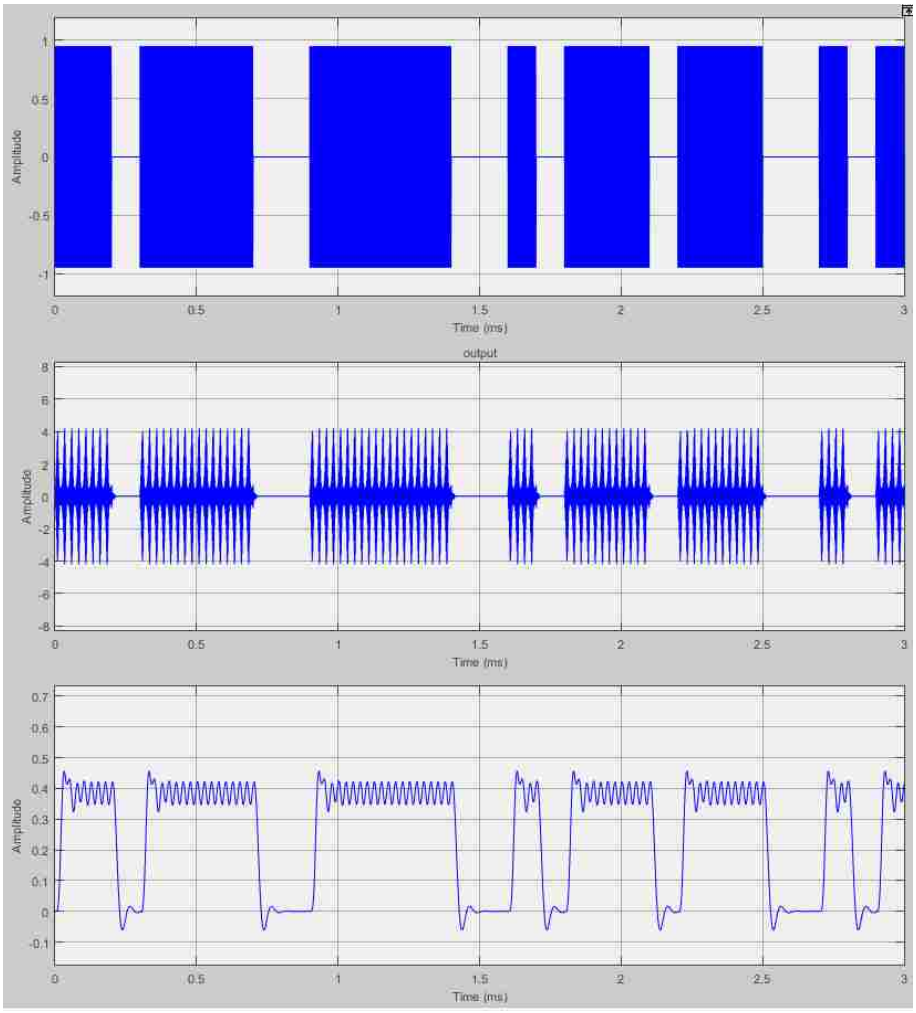

Figure 4-2. Simulation of Ideal SRR: (a) RF Input (b) SRO Output (c) Envelop Detector.

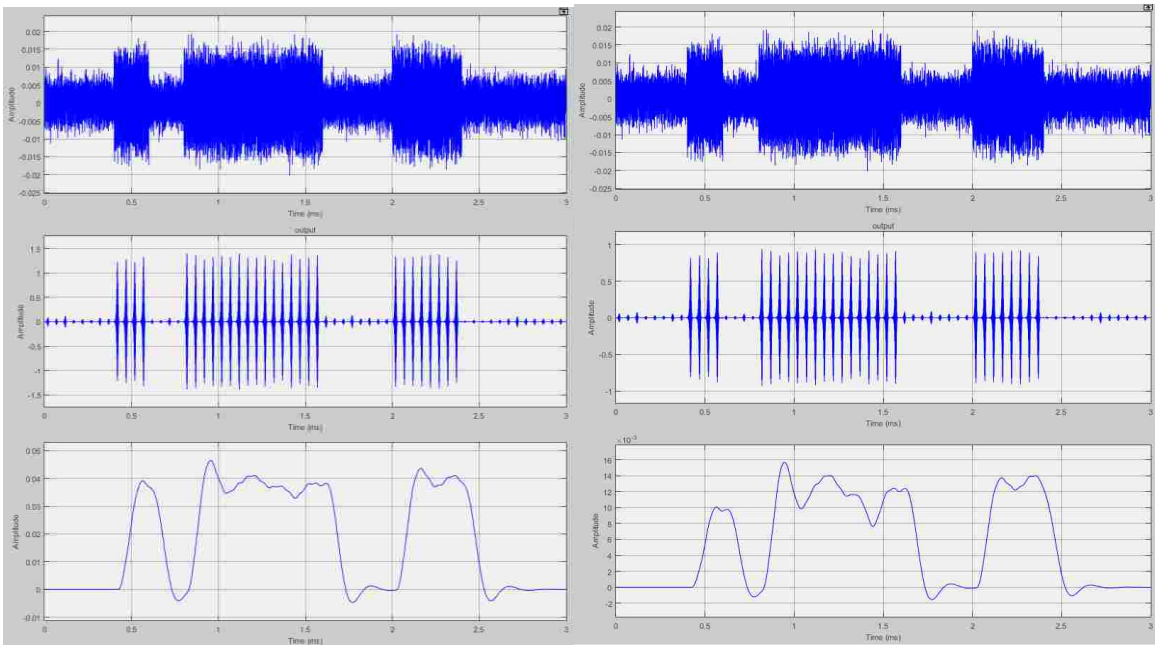

Figure 4-3. Simulation Results Given: Ko=1.5, Ka = 1 (Left) and Ka= 1.5, Ko = 1 (Right).

4.3 Multiple Resonance Due to Increasing Quench Frequency

The following results in Figure 4-4 demonstrate the effects on the frequency response of the system in the sinusoidal steady state by raising the quench frequency while keeping all other parameters constant. Figure 4-4a is the frequency response of our original simulation. Figure 4-4(b-d) are the resulting frequency responses from increasing the quench frequency. As expected, the gain decreases as the quench frequency increases due to the lower amount of high frequency RF cycles within a single quench period. It is also apparent that increasing the quench frequency while keeping the DC component of the damping function constant accentuates the multiple resonance effect due to hangover discussed in section 3.4. Each resonant peak occurs at an integer multiple of the quench frequency away from the tuned center frequency of the system.

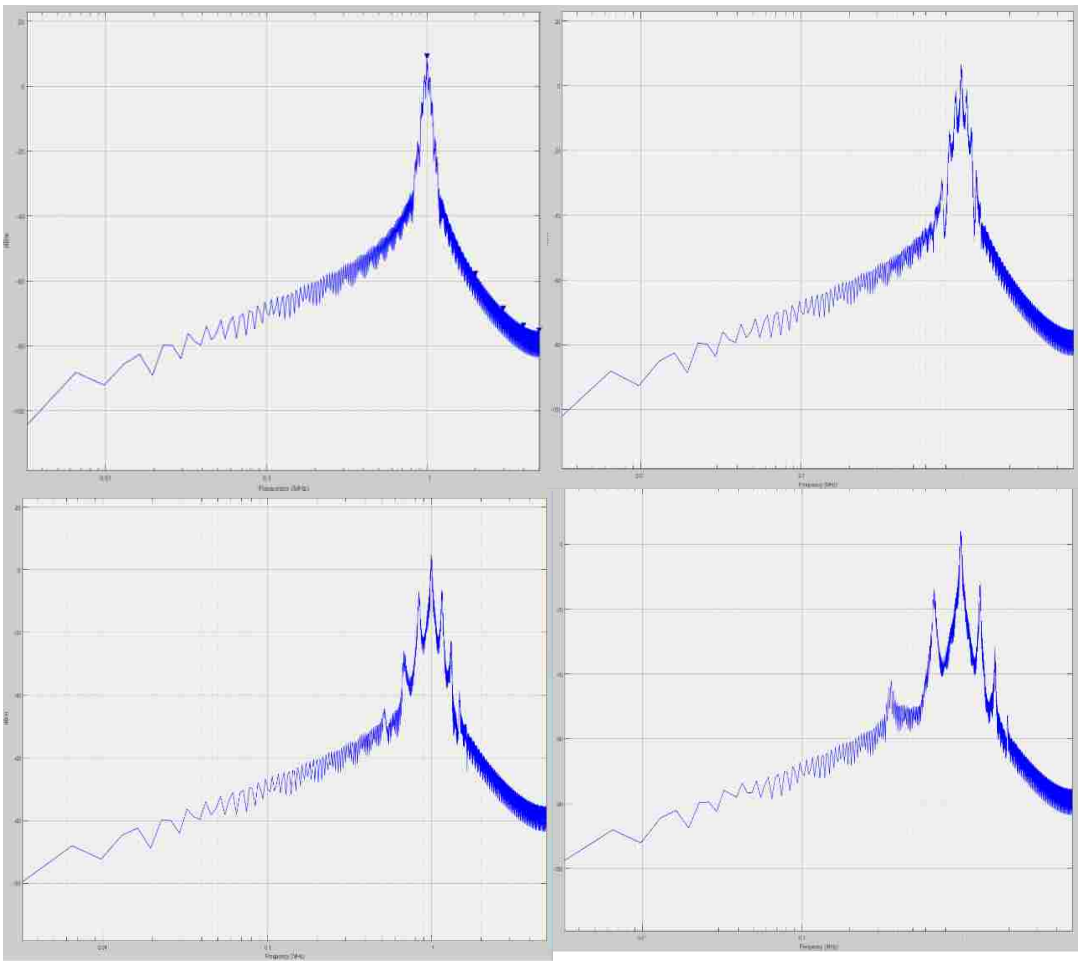

Figure 4-4. Example of Multiple Resonance: (a) $f_q = 40\ KHz$ (Top Left), (b) $f_q = 80\ KHz$ (Top Right), (c) $f_q = 160\ KHz$ (Bottom Left), (d) $f_q = 320\ KHz$ (Bottom Right).

4.4 Hangover Due to Reducing the Quiescent Damping Factor

Figure 4-5 consists of two simulations that demonstrate the hangover effect due to a reduction of the quiescent damping factor ζ_0. The response in (a) is an expected output for a system whose damping factor is kept high enough such that the oscillations are adequately quenched. The response after decreasing ζ_0 by a factor of 2 while keeping all other parameters constant is shown in (b). First note that this results in a significant gain reduction, as both regenerative and super-regenerative gains are exponentially related to

the area enclosed by one cycle of the damping function. This reduction also drastically effects the system's ability to extinguish oscillations after an RF input ceases. If this single pulse was instead a digital bit stream or a series of pulses, the hangover in (b) would cause the comparator portion of the detector to falsely output a logical HIGH value despite receiving a logical LOW input at that instance of time.

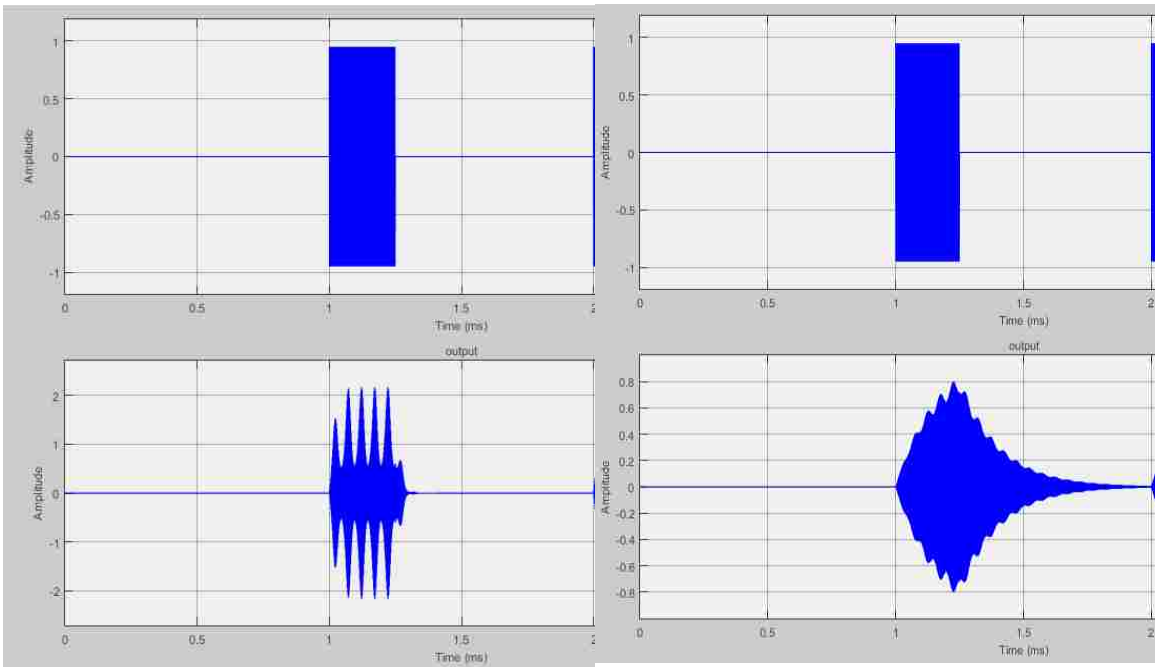

Figure 4-5. SRR response to an input RF pulse given a high (left) and low (right) quiescent damping factor.

4.5 Simulation with an Amplitude Modulated Input Signal

The simulations in this section are intended to provide a closer representation to the practical design that will be proposed in Chapter 5. To mimic the electrical limitations of the time-varying gain element used in the practical design, a saturation block was inserted before multiplication that clips the quench signal for values larger than +/-

50mV. Since the feedback gain can no longer be controlled by arbitrary quench signal values (which previously corresponded to K_a), two amplifiers with gains of 10 V/V were added to the feedback path and at the SRO output to compensate for the gain reduction. These modifications to the original simulation model are shown in Figure 4-6.

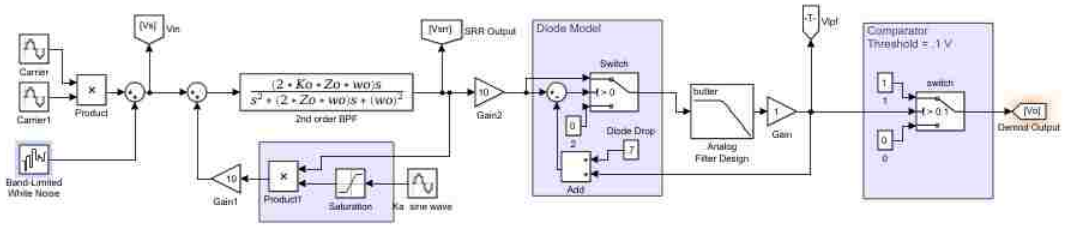

Figure 4-6. Modified SRR Model.

The input signal is a noisy AM waveform obtained from the product of a 20 KHz sinusoidal message signal of 500mVac with a 1Vdc bias and a 1 MHz, 100mVac carrier wave. These values were chosen to represent a typical AM input signal at the maximum audible frequency that a practical SRR may receive, demonstrating its suitability for receiving continuous AM audio signals.

Two simulations were conducted using different quench signal amplitudes to demonstrate the linear and saturated operating modes of the practical time-varying gain element. The first simulation shown in Figure 4-7 is resultant of a 60 KHz, .05Vac sinusoidal quench signal controlling the feedback gain of the SRO. In this case, the sinusoidal quench signal controls the gain linearly as it did in previous simulations. From top to bottom, the graphs in Figure 4-7 depict the input AM waveform, the output of the SRO and the output of the envelope detector with a low pass filter cutoff frequency of 25 KHz.

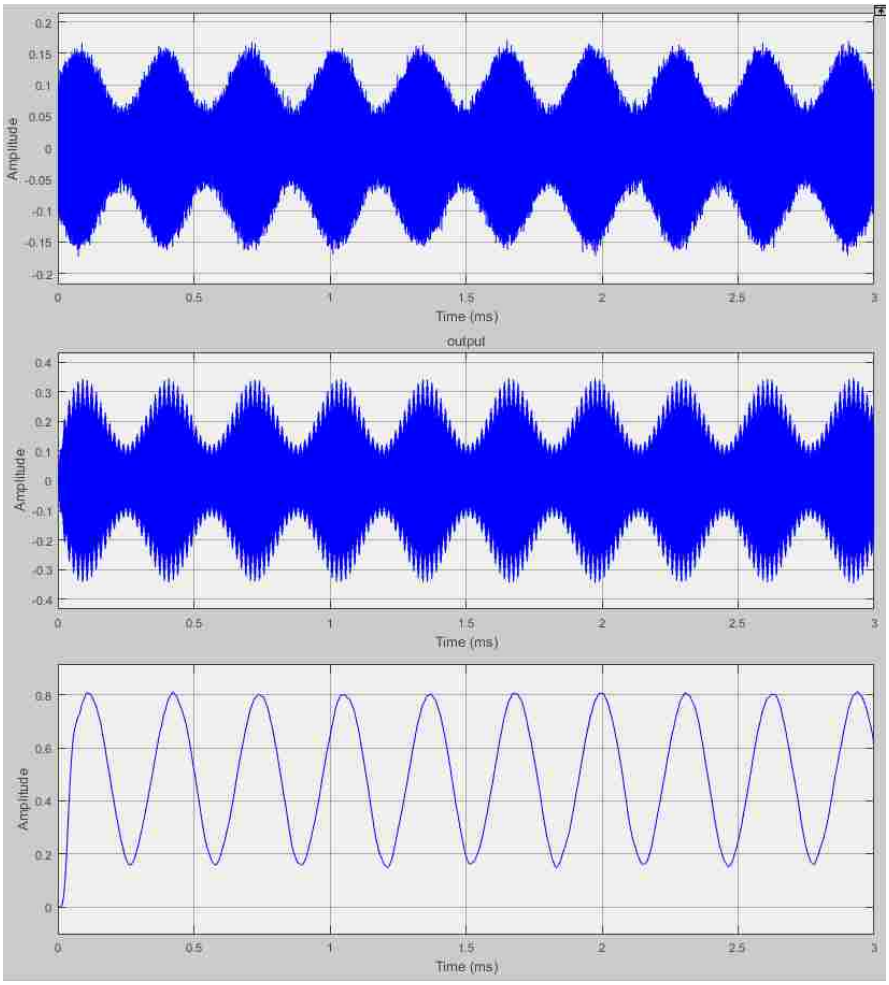

Figure 4-7. SRR Simulation with an AM Input Signal and Linear Gain Control: (a) AM Input Signal (Top), (b) SRO Output (Center), (c) Envelope Detector Output (Bottom).

The second simulation shown in Figure 4-8 is resultant of a 60 KHz, .2Vac sinusoidal quench signal that exceeds the imposed 50mV saturation limit of the gain element. The clipping of this control signal results in the square wave damping function depicted in the upper plot of Figure 4-8. The center and bottom plots again depict the SRO output and envelope detector output respectively.

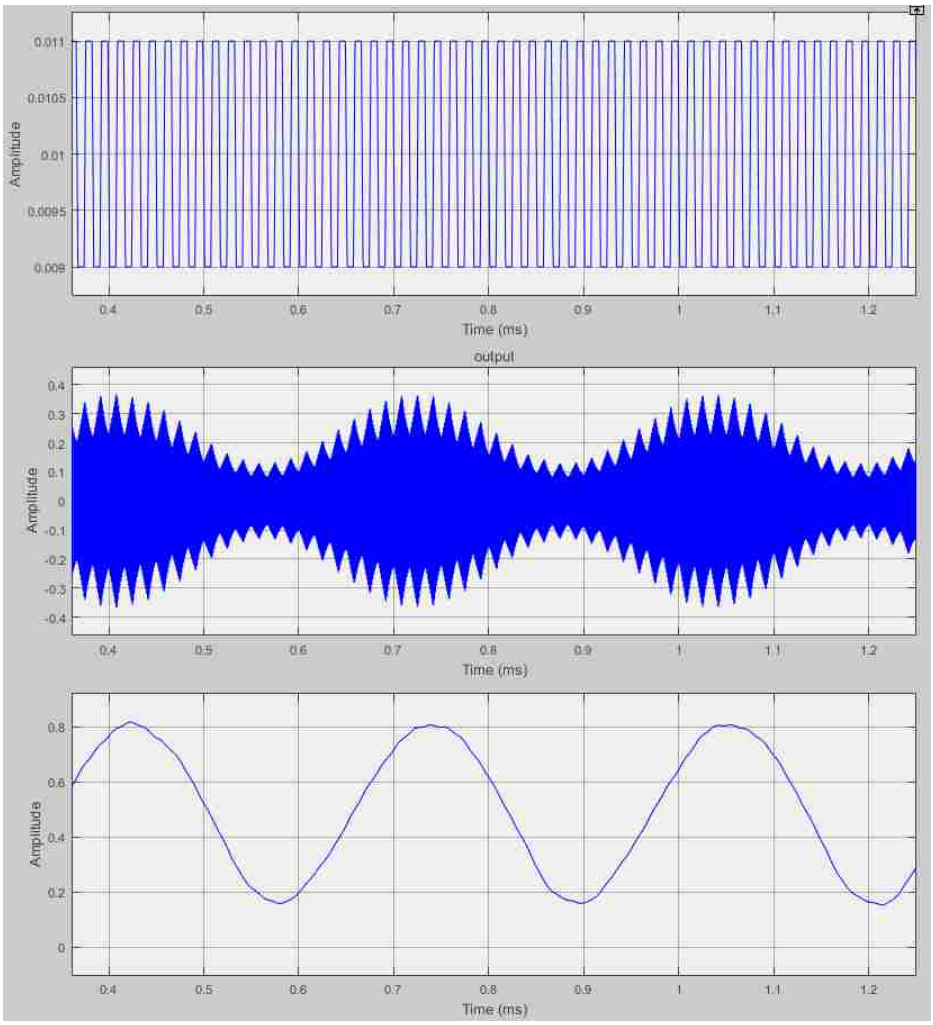

Figure 4-8: SRR Simulation with an AM Input Signal and Saturated Gain Control: (a) damping function (top), (b) SRO Output (Center), Envelope Detector Output (Bottom).

Not only do these simulations demonstrate the SRRs ability to demodulate practical continuous signals, but they also prove that both sinusoidal and square quench signals (and thus, sinusoidal and square damping functions) can be used to control the feedback gain of the SRR with similar results. This fact reiterates the comments made in Section 3.2 that the shape of the damping function is arbitrary so long as the system is designed to have appropriate durations of sensitivity, regeneration and quenching.

Chapter 5

Electrical Model & Practical Implementation

5.1 Electrical Model

Now that a strong mathematical understanding of SRR operation has been established, the generic results of previous sections can be easily applied to an electrical model. Figure 5-1 presents the most common electrical representation to model super-regenerative operation.

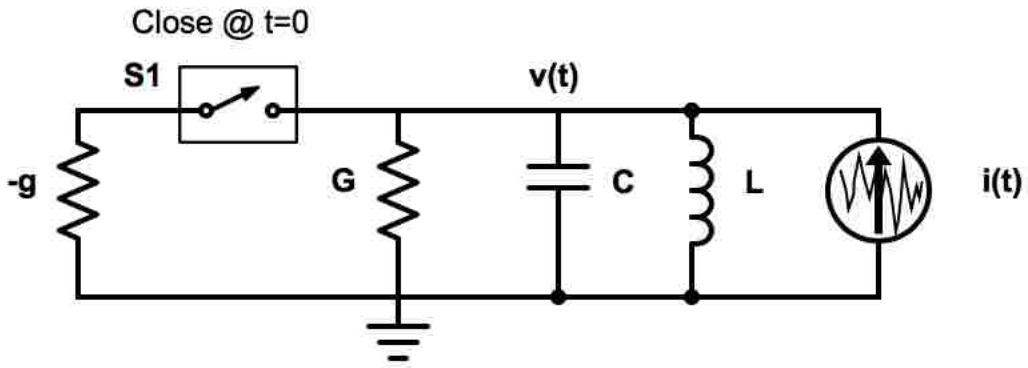

Figure 5-1. Electrical Model of a Super-Regenerative Receiver.

This circuit is simply an LC tank circuit with an added conductance G that models the tank's resistive losses, and a time-varying negative conductance g in parallel with the tank's inherent conductance. The RF current source $i(t)$ represents incoming external RF signals induced in the tank, which can be thought of as the signal from a receiving antenna represented as

$$i(t) = A(t)sin(\omega_0 t). \tag{5.1}$$

Since we are interested in the operation of the receiver when it is tuned to the input carrier frequency, we shall assume that $\omega_c \approx \omega_0 = \sqrt{\frac{1}{LC}}$ as defined in [5].

When the switch is open ($t < 0$), the voltage across the tank takes on the expression

$$v(t) = v_o k e^{-\frac{tG}{2C}} * \sin(\omega_0 t). \tag{5.2}$$

When the switch closes ($t \geq 0$), the negative conductance g is added to the tanks quiescent conductance G. To simplify the analysis, we shall assume that the total conductance of the network is equal to some positive value G when the switch is open, and some new negative value $-g$ when the switch is closed. Once the switch is closed, the equation describing the circuit via KCL is

$$C\dot{v} + gv + \frac{1}{L}\int_0^t v dt = i(t). \tag{5.3}$$

The solution in terms of the tank voltage is then given as

$$v(t) = v_o k e^{+\frac{tg}{2C}} * A(t)\sin(\omega_0 t) \tag{5.4}$$

$$\omega_0 = \sqrt{\frac{1}{LC} + \left(\frac{g}{2C}\right)^2} \tag{5.5}$$

As can be seen from (5.4) when the negative conductance is introduced the voltage across the tank is sinusoidal with an exponentially increasing amplitude envelope. Relating this to the generic closed loop model, the damping factor of this system at this particular instant is less than or equal to 0, meaning the system is undamped and the amplitude of oscillations will rise to ever-increasing levels due to positive feedback. In practical cases, non-linearities of oscillatory circuits will cause the amplitude to level off over time, making the network a steady oscillator of constant amplitude. However, for the purposes of this example it is assumed that the switch will open before the oscillations

reach a steady amplitude, thus preserving the receivers' linear mode of operation. It should be noted from (5.4) that introducing a negative conductance will shift the center frequency of the band pass network, and so the magnitude of this additional term should be kept small enough to minimize its effects on the center frequency.

When the switch opens again, the voltage across the tank reverts back to a decaying sinusoid approaching 0V. Since the state of the switch is dictating weather the network is overdamped (open) or undamped (closed), this hard switching scheme is equivalent to a square wave quench signal controlling the feedback gain of our generic model, alternating the network between stable and unstable states. The switching period is equivalent to the quench period of the quench oscillator (and thus, the period of the time-varying feedback gain). With this in mind, the switching action of this band pass network can be modeled as a time-varying conductance in parallel with the networks inherent conductance.

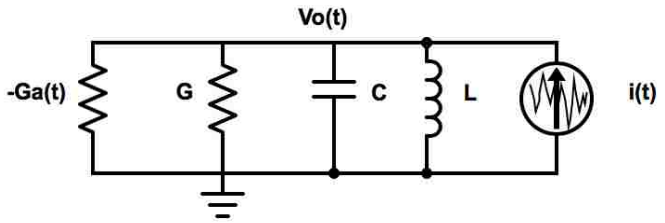

Figure 5-2. Electrical Model with a Time-Varying Conductance.

From this form, all of the general parameters from Chapter 3 can be mapped to equivalent electrical parameters which would provide the same mathematical results from an electrical perspective as shown in [10] and [12]. Mappings of these parameters are given in Table 5-1.

	Block Diagram	Electrical Model
Input Signal	v_{in}	i
Output Signal	v_o	v_o
Tuned Frequency	ω_0	$\frac{1}{\sqrt{LC}}$
Filter Gain	K_0	$Z_0 = \frac{1}{G_0}$
Damping Ratio	ζ_0	$\frac{1}{2R_0 C\omega_0} = \frac{1}{2Q_0} = \frac{Z_0}{2R}$
Feedback Gain	$K_a(t)$	$G_a(t)$
Damping Function	$\zeta(t) = \zeta_0[1 - K_a(t)K_0]$	$\zeta(t) = \zeta_0[1 - G_a(t)Z_0]$

Table 5-1. Parameter Mappings for the Equivalent Electrical Model

5.2 Self-Quenching

As mentioned earlier, quenching can be achieved externally with an oscillator controlling the feedback gain, or by designing the band pass network to allow for "self-quenching." In fact, a large reason why supper-regenerative receivers were popular in the earlier years of communications was because non-linear characteristics of a single device (transistor or tube) could be exploited to detect and perform self-quenching at the same time, reducing the cost and size of the circuit (an attractive benefit considering the size of transistors and tubes at the time).In practice, the transistor acts as a nonlinear negative resistance, providing the oscillatory response described for the simple RLC circuit above.

5.3 Colpitts Oscillator

As a practical example, the single-transistor SRR design presented in [5] shall be considered. The core of the receiver discussed in [5] is based on the simple yet popular Colpitts oscillator shown in Figure 6-3. The gain element is a bipolar transistor amplifier in a common emitter configuration. Rb1 and Rb2 bias the transistor. Resistor R_c limits

the collector current of the transistor. Capacitors C_{in} and C_{out} act as decoupling capacitors to separate and remove the DC component of the AC signal. Capacitor C_e acts as an emitter bypass capacitor that prevents the amplified AC from dropping across R_e. Without it, the AC signal will drop across R_e and alter the DC biasing conditions of the Amplifier.

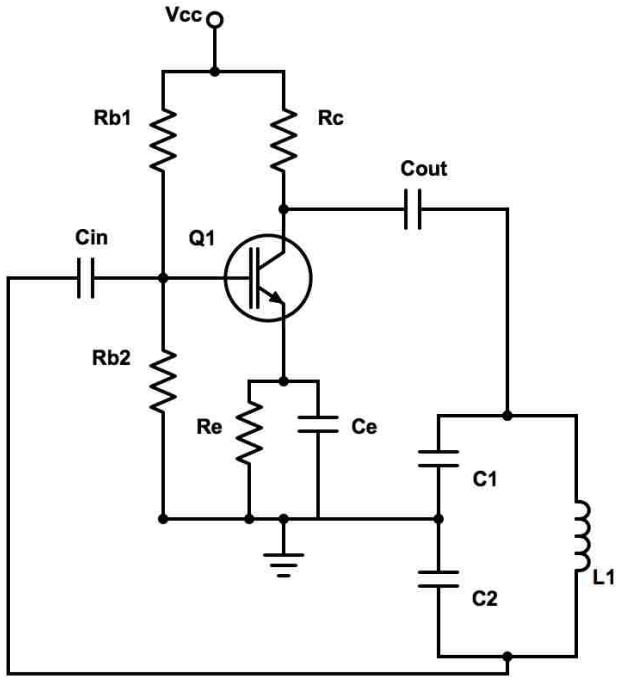

Figure 5-3. Colpitts Oscillator.

The output at the collector is fed back to the base with a resonant LC tank circuit in the feedback loop. The two capacitors in the tank form a single "tapped" capacitor whose total effective capacitance is determined by

$$C_{total} = \frac{C_1 C_2}{C_1 + C_2} \tag{5.6}$$

When the power is switched on, the capacitors in the tank start charging. When fully charged, they start to discharge through the tanks inductor L. When the capacitors fully discharge, the stored electrostatic energy is transferred as magnetic flux through the

inductor. Once the inductor starts discharging its energy, the capacitors charge up again. The energy transfer between these elements form the basis of the circuits oscillation. The frequency of oscillation is characterized by the equation

$$f = \frac{1}{2\pi\sqrt{LC_{total}}} \tag{5.7}$$

In a passive tank circuit, these oscillations will eventually die out as the reactive elements reach steady state equilibrium. To sustain oscillations, the lost energy is compensated by the common-emitter transistor amplifier. This amplifier configuration takes an input signal at the base and outputs a scaled version of the signal shifted 180° at the collector output. Grounding the connection between C1 and C2 results in equal voltages of opposite polarity across the two elements, thus introducing another 180° phase shift such that the feedback signal is in-phase with the input. The resulting positive feedback sustains the oscillations at an amplitude level characterized by component values of the amplifier. The author of [5] modifies the base-emitter junction of this steady oscillator with an added RLC circuit to achieve time-varying gain resulting in self-quenching operation.

5.4 Alternative Time-Varying Gain Element

The initial goals for the practical design offered in this section were focused on modifying the single-transistor Colpitts oscillator to achieve self-quenching operation with minimal additional components, all while maintaining suitable performance within the AM frequency range. Unfortunately, the non-linear gain control of the single-transistor design could only be partially described by the analysis presented in Chapter 3. To conclude the concepts and analysis of this report, this section presents a practical

implementation that utilizes a monolithic IC package to realize the time-varying gain element of the SRO model. Though this modification sacrifices cost efficiency, it allows for a circuit realization that is closely related to the simulation model presented in Section 4.

Much like the simulation model, this circuit consists of a selective network whose output is fed back to an MC1496 monolithic balanced modulator which is configured to act as the externally controlled amplifier in

Figure 1-1. The schematic for the MC1496 is shown in Figure 5-4. The design consists of a differential amplifier (Q5-Q6) that drives a dual differential amplifier pair (Q1-Q2, Q3-Q4). Transistors Q7 and Q8 and connecting bias circuitry form two DC current sources to provide proper biasing of the lower differential pair. This circuit topology is identical to the four-quadrant multiplier discussed in [13], and is characterized by its ability to deliver an output that is proportional to the product of two input signals. As a four-quadrant multiplier, the MC1496 permits multiplication of both positive and negative input signals, making it an effective building block for numerous RF applications of varying complexity. The schematic shown in Figure 5-5 is a simplified model to demonstrate and analyze the performance of a four-quadrant multiplier. Note that the additional emitter and load resistors R_E and R_L are external components used to set the appropriate device voltage gain for the design application.

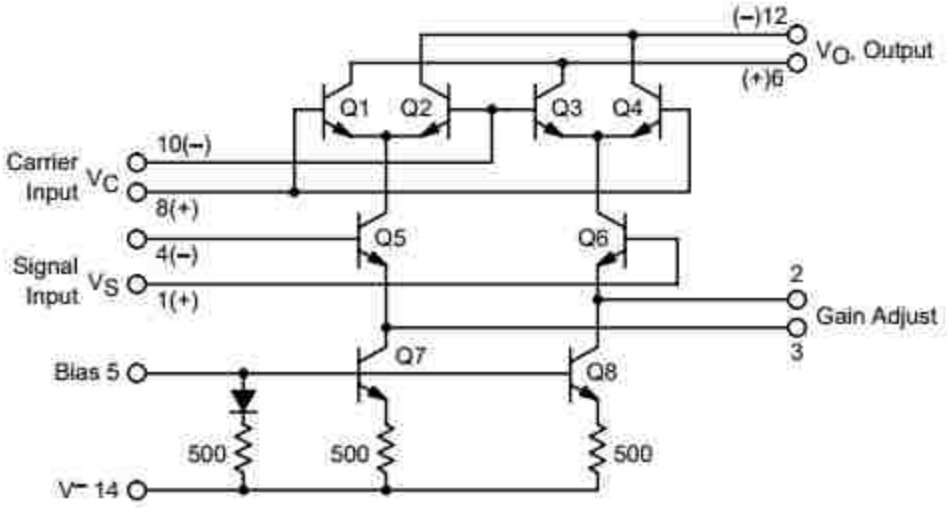

Figure 5-4. Schematic of MC1496 Balanced Modulator.

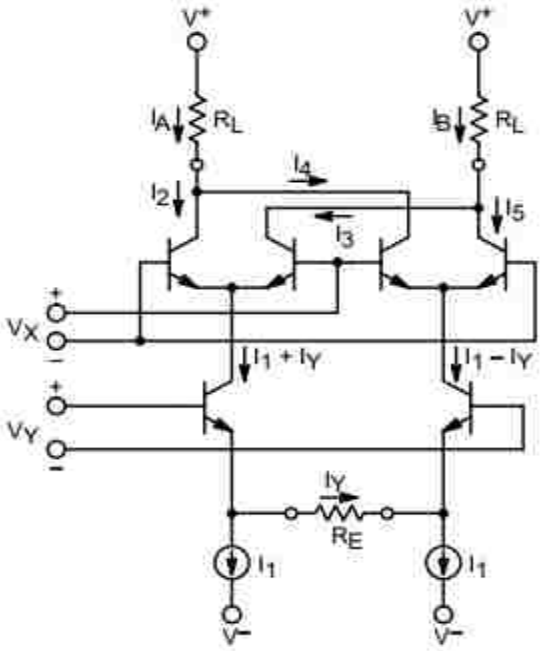

Figure 5-5. Analysis Model for the MC1496.

Analysis of the multiplier circuit is based on the assumption that the BJT pairs are matched and have negligible base currents. Under this assumption, the following expressions for the branch currents can be defined:

$$I_1 = I_5 \equiv I_{bias} \tag{5.8}$$

$$I_y = \frac{V_y}{R_E} \quad (R_E \gg r_e) \tag{5.9}$$

$$\left.\begin{aligned} I_2 &= \frac{(I_1+I_y)}{1+e^{\frac{V_x}{a}}}, \quad I_3 = \frac{(I_1+I_y)}{1+e^{-\frac{V_x}{a}}} \\ I_4 &= \frac{(I_1-I_y)}{1+e^{-\frac{V_x}{a}}}, \quad I_5 = \frac{(I_1-I_y)}{1+e^{\frac{V_x}{a}}} \end{aligned}\right\} \tag{5.10}$$

Where

$$a = \frac{kT}{q} \qquad . \tag{5.11}$$

Currents I_A and I_B can be represented as sums of these collector currents,

$$\left.\begin{aligned} I_A &= I_2 + I_4 = \frac{(I_1+I_y)}{1+e^{m}} + \frac{(I_1-I_y)}{1+e^{-m}} \\ I_B &= I_3 + I_5 = \frac{(I_1+I_y)}{1+e^{-m}} + \frac{(I_1-I_y)}{1+e^{m}} \end{aligned}\right\} \tag{5.12}$$

where $m = \frac{V_x}{a}$. Taking the difference between Currents I_A and I_B as derived in [14] yields

$$I_A - I_B = \frac{2I_y(e^{-m}-e^{m})}{(1+e^{m})(1+e^{m})}. \tag{5.13}$$

The differential voltage between the two load resistors is then given as

$$\Delta V_o = R_L \frac{2I_y(e^{-m}-e^{m})}{(1+e^{m})(1+e^{m})}. \tag{5.14}$$

Combining (5.9) with (5.14) and substituting $\frac{V_x}{a}$ back into the equation forms for the complete expression for the voltage gain from the differential output to input V_y

$$\frac{\Delta V_o}{V_y} = \frac{2R_L}{R_E} \frac{(e^{-\frac{V_x}{a}}-e^{\frac{V_x}{a}})}{(1+e^{\frac{V_x}{a}})(1+e^{-\frac{V_x}{a}})} = -\frac{2R_L}{R_E}\tanh(\frac{V_x}{2a}) \tag{5.15}$$

From this expression it can be seen that the voltage gain is a non-linear function of the input signal applied to the upper two differential pairs. The hyperbolic tangent function in (5.15) is approximately linear for argument values close to zero and levels off to +/- 1 as the argument departs further from zero. A large sinusoidal control voltage would appear

as a square wave periodically changing the sign of the input voltage. Alternatively, a low voltage control signal can be used to vary the voltage gain linearly, causing the multiplier to act as a variable gain amplifier. The amplitude limits imposed on the applied control voltage signal for linear operation are further defined in [14], though the typical range is +/- 50mV.

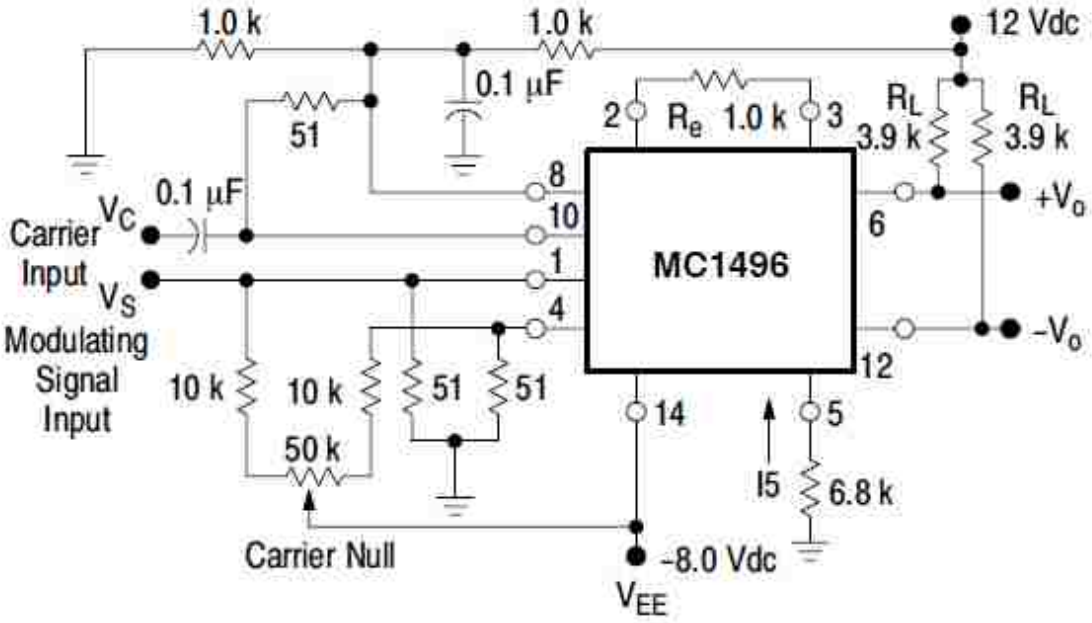

Figure 5-6. Balanced modulator configuration.

Figure 5-6 depicts the typical configuration for the balanced modulator as provided by the MC1496 datasheet [14]. The gain element of the SRO will be implemented using this configuration with a few changes to the defined inputs. The output voltage v_0 of the selective network will be fed into input V_S (V_y) and the external quench signal v_q will be applied to input V_c (V_x). The differential output of the MC1496 will feed into a differential amplifier, converting it into a single ended signal to be fed back to the selective network input.

5.5 Proposed Design & Implementation

The schematic of the proposed SRR design for circuit simulation is shown in Figure 5-7. Three voltage sources fed into an operational amplifier are used to model a 300mV AM signal with a carrier frequency of 1 MHz and message frequency of 20 KHz. The band pass filter is composed of the simple LC tank that is used as the selective network for the Colpitts oscillator. The variable gain amplifier mimics the MC1496 circuit schematic in Figure 5-4 with the appropriate connections for a balanced modulator as given in Figure 5-6. The applied quench signal to the MC1496 is a 50mV sinusoid with a frequency of 120 KHz. 60 KHz was sufficient for the ideal model simulated in Matlab, however this frequency did not provide sufficient quenching in the practical design. The differential output is fed into a differential amplifier to provide voltage gain and convert the output to a single ended voltage signal which feeds back to the selective network. The peak detector circuit is designed to have a time constant sufficient for reasonable tracking of the output envelope and is cascaded with a low pass filter with a cutoff frequency of around 30 KHz to reduce the rippling effect from the quenched output pulses.

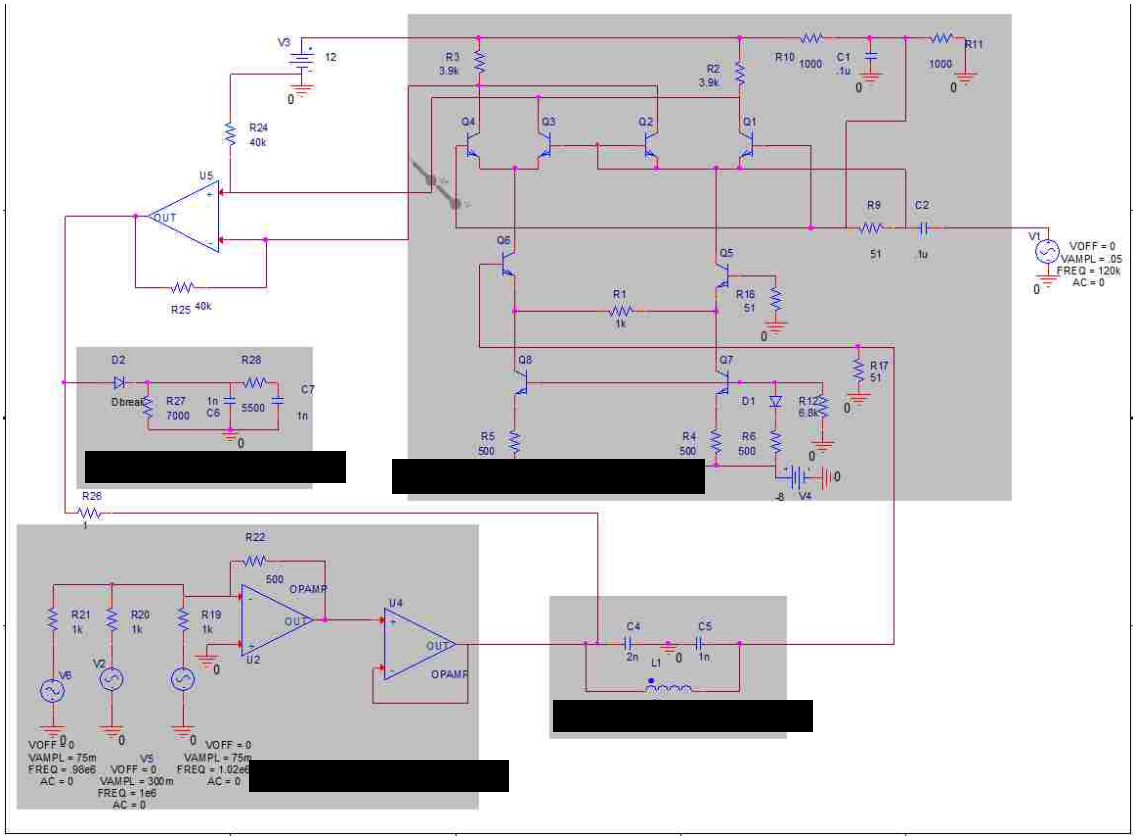

Figure 5-7. Schematic of the Practical SRR Implementation

The simulation results of this circuit are shown in Figures 5-8. The blue and red signals in Figure 5-8a are the input AM signal and the output of the amplifier in the feedback loop respectively. The quenching action of the feedback amplifier becomes apparent after 200μs as the pulses occurring every T_q seconds become more defined. Figure 5-8b is a magnified view of 5-8a starting at 200μs to provide a clearer view of the output pulses. Figure 5-8c depicts the output of the peak detector circuit compared to the input signal. As can be seen, the peak detector accurately tracks the quenched output pulses and successfully extracts the 20 KHz message signal from the modulated carrier with a 500mVdc offset.

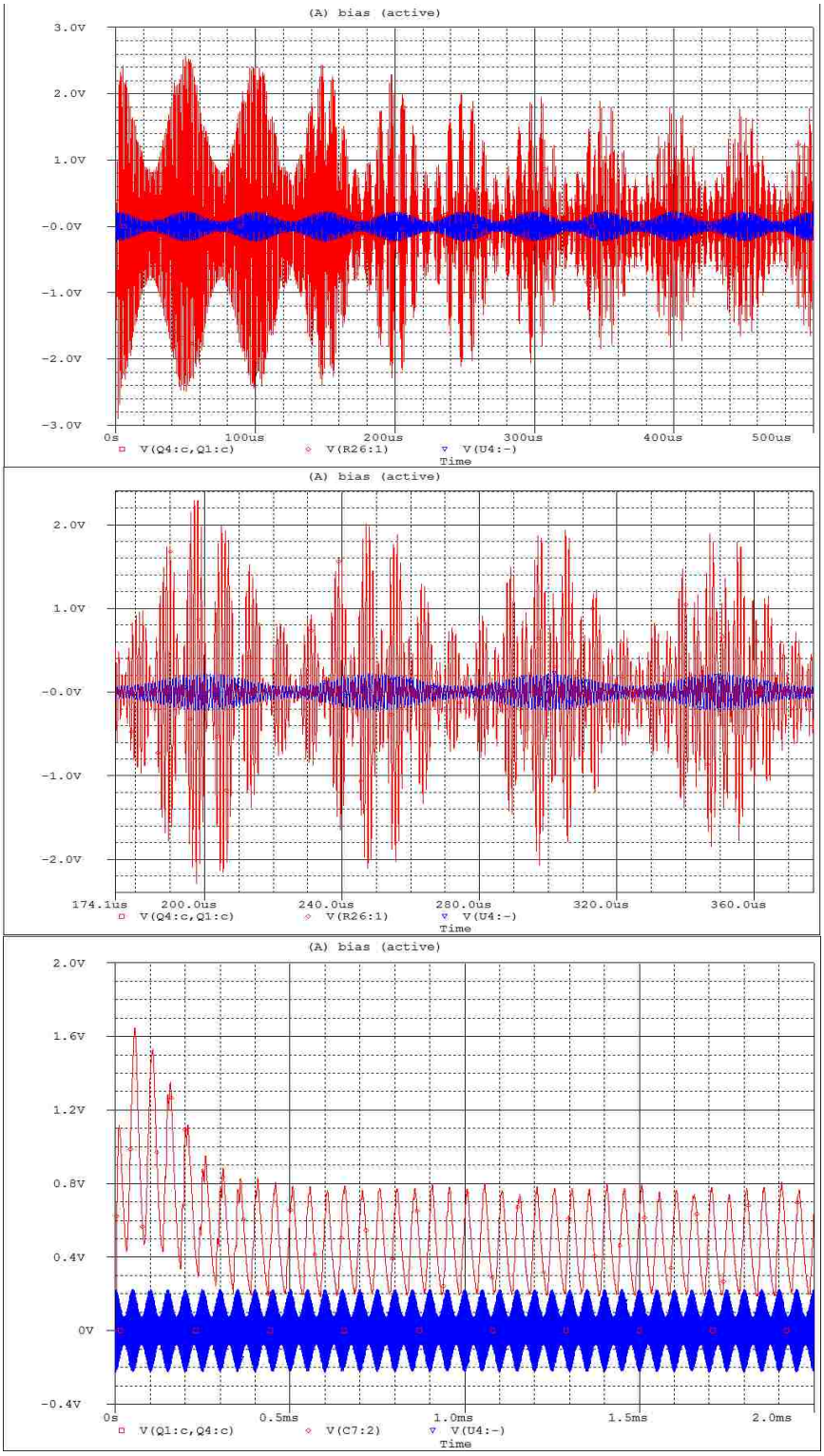

Figure 5-8. (a) Feedback Amplifier Output (Top), (b) Magnified View of Feedback Amplifier Output (Center), (c) Peak Detector Output (Bottom).

5.6 Physical Implementation

A physical prototype of the simulated design is given in Figure 5-9. The selective network and MC1496 are configured as they were in the simulation, however some minor adjustments were made to account for the non-idealities of the practical op-amp used to amplify the feedback signal after multiplication. Instead of sending both outputs of the MC1496 to a differential amplifier, this circuit feeds a single-ended output to a pair of cascaded HA-2515 op-amps in non-inverting configuration. The HA-2515 has a gain-bandwidth product of 12 MHz which is higher than typical operational amplifiers. However, a considerable amount of amplification was needed to boost the low-voltage single-ended signal from the balanced modulator. The cascaded design ensures sufficient amplification for peak detection can be achieved while still preserving the integrity of the signal.

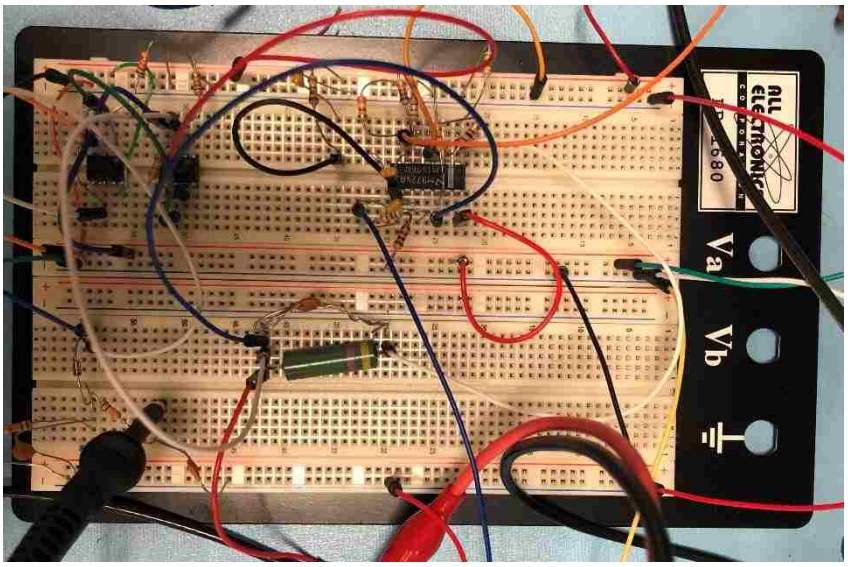

Figure 5-9. Prototype of the proposed SRR design.

The results of this circuit configuration are shown in Figure 5-10. The input signal is a 300mVac 1 MHz AM signal modulated by a 20 KHz message signal. The quench signal is a 60mVac sinusoid with a frequency of 120 KHz. Like the simulated design, a quench frequency of 60 KHz did not extinguish the building oscillations sufficiently, which compromised the envelope of the 20 KHz message signal. The 150mV signal in Figure 5-10a is the single-ended output of the MC1496. The quenched pulses in the output waveform are comparable to those shown in Figure 5-8. This signal was fed into two cascaded non-inverting op-amps, each providing a gain of roughly 5.2 V/V using 39 KOhm and 8.2 KOhm resistors. The feedback signal before and after amplification is compared in Figure 5-10b by the yellow and blue signals respectively. The 4V signal after amplification is sent to the peak detector circuit previously discussed in Section 2.3 which is cascaded with a low pass filter. The parallel configuration of the 1nF capacitor and 18.9 KOhm has a time constant of 18.9μs (52.9 KHz) which allows the peak detector the track the envelope of the 120 KHz output pulses effectively. The passive RC low pass filter has a cutoff frequency of 100 KHz to remove some of the ripple caused by the high frequency pulses. A comparison of the amplified feedback signal and the output signal of the peak detector is given in Figure 5-10c. As can be seen, the SRR circuit successfully demodulates the 1 MHz AM signal and outputs the extracted 20 KHz message signal. Depending on the requirements of the application, further amplification and higher order filtering can be implemented after demodulation to boost the signal strength and improve the integrity of the sinusoid.

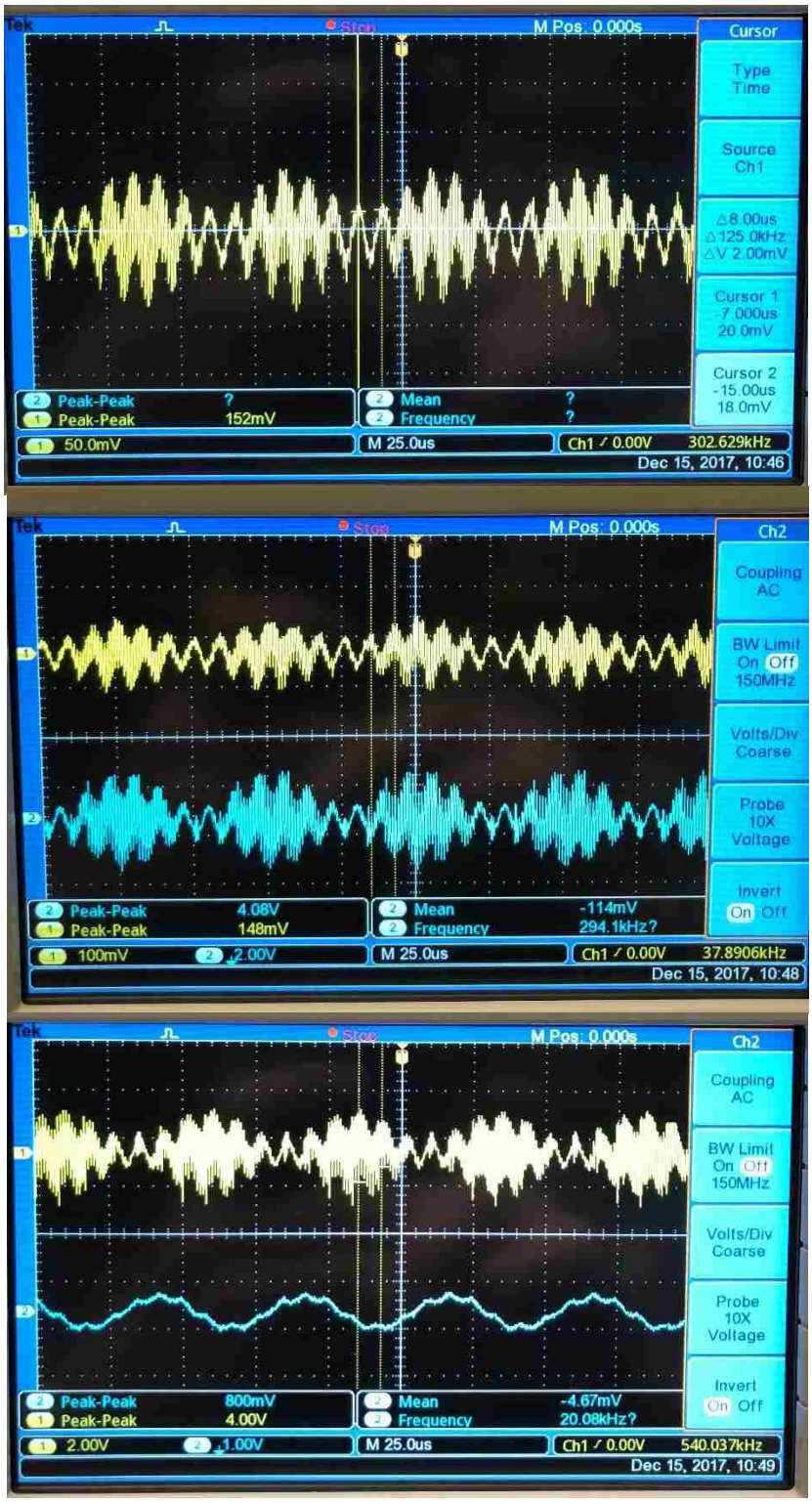

Figure 5-10. (a) Output of MC1496, (b) feedback signal before and after amplification, (c) peak detector output compared to amplified feedback signal.

Chapter 6

Conclusions & Future Work

Despite their age, Super-Regenerative Receivers have proven to be resilient options for RF reception in applications where low-power consumption, architecture simplicity and cost efficiency are desired. This study has successfully presented a mathematical understanding of SRR operation and working implementation to demonstrate the theoretical results. Though the final design deviated from the initial goal of minimizing cost and complexity, it boasts an architecture that is easily relatable to the generic model that has been used to understand SRR operation for decades. The generic mathematical analysis and the easily relatable practical implementation can be used as a springboard for improved SRR architectures designed for specifically for various communication applications.

Future work will focus on integrating the self-quenching action described in Chapter 6 into the current design. The intent of this modification is to allow for optimal quenching frequencies across a range of desired carrier frequency inputs without the need for an externally controlled oscillator. This improvement would benefit commercial radio receivers that are expected to operate consistently across numerous frequency bands in the AM and FM range.

With the increasing relevance of short range communications for RFID and sensor network applications, integrating the proposed design into a single package via CMOS technology is also worth considering. Such applications include the Internet of Things, home automation and remote control operation of consumer devices. The design of sensors and RFID tags is highly focused on minimizing the size and power of the

device so that they are non-intrusive and have a long battery life. These devices typically do not require high-level performance, making the SRR a highly affordable option for the intended communication purposes. Integrating the proposed design into a smaller package would make for an attractive option as the need for smaller, long-lasting RF communication devices continues to grow.

References

[1] Moncunill-Geniz, F., Pala-Schonwalder, P., & Mas-Casals, O. (2005). A generic approach to the theory of superregenerative reception. IEEE Transactions on Circuits and Systems I: Regular Papers, 52(1), 54-70

[2] Vouilloz, A., Declercq, M., & Dehollain, C. (n.d.). Selectivity and sensitivity performances of superregenerative receivers. ISCAS 98. Proceedings of the 1998 IEEE International Symposium on Circuits and Systems.

[3] Lee, D., & Mercier, P. P. (2017). Noise Analysis of Phase-Demodulating Receivers Employing Super-Regenerative Amplification. IEEE Transactions on Microwave Theory and Techniques.

[4] Hernandez, L., & Paton, S. (n.d.). A superregenerative receiver for phase and frequency modulated carriers. 2002 IEEE International Symposium on Circuits and Systems. Proceedings.

[5] Insam, E. (april 2002). Designing Super-Regenerative Receivers. Electronics World.

[6] Frey, D. R. (2013). Improved Super-Regenerative Receiver Theory. IEEE Transactions on Circuits and Systems.

[7] Frey, D. (2006). Synchronous filtering. IEEE Transactions on Circuits and Systems.

[8] Pala-Schonwalder, P., Moncunill-Geniz, F. X., Bonet-Dalmau, J., Del-Aguila-Lopez, F., & Giralt-Mas, R. (2009). A BPSK superregenerative receiver. Preliminary results. 2009 IEEE International Symposium on Circuits and Systems.

[9] Lathi, B. P. (2016). Signal processing and linear systems. New York: Oxford University Press.4]

[10] Thoppay, P. E., Dehollain, C., & Declercq, M. J. (2008). Noise analysis in super-regenerative receiver systems. 2008 Ph.D. Research in Microelectronics and Electronics.

[11] Feick, R., & Rojas, O. (1997). Modeling and simulation of the superregenerative receiver. IEEE Transactions on Consumer Electronics.

[12] Bonet-Dalmau, J., Moncunill-Geniz, F. X., Pala-Schonwalder, P., Aguila-Lopez, F. D., & Giralt-Mas, R. (2012). Frequency Domain Analysis of Superregenerative Receivers in the Linear and the Logarithmic Modes. IEEE Transactions on Circuits and Systems.

[13] Franco, S. (2015). Design with operational amplifiers and analog integrated circuits. New York: McGraw-Hill.

[14] ON Semiconductor (October, 2006). Balanced Modulators/Demodulators. MC1496.

Biography

Anthony Evelina was born on November 19th, 1993. He lives in Caldwell, New Jersey with his parents Darlene and Robert Zalewski, and his grandmother Marie Lanfrank. Anthony attended Montclair Kimberley Academy from kindergarten until his high school graduation in May 2012. After graduation, he attended Lehigh University to pursue a degree in Electrical Engineering. After graduating with a B.S. in Electrical Engineering in May 2016, he continued his studies at Lehigh to work towards a M.S. in Electrical Engineering and is expected to complete the requirements by December 2017. During his time as a graduate student, Anthony served as a Teacher's Assistant for the 2016-17 ECE 258 Senior Design Class and as an Adjunct Lecturer for the ECE 182 Junior Lab in the summer of 2017. Outside of engineering, Anthony has enjoyed playing the guitar for ten years and he has actively performed with two jazz bands at Lehigh University.